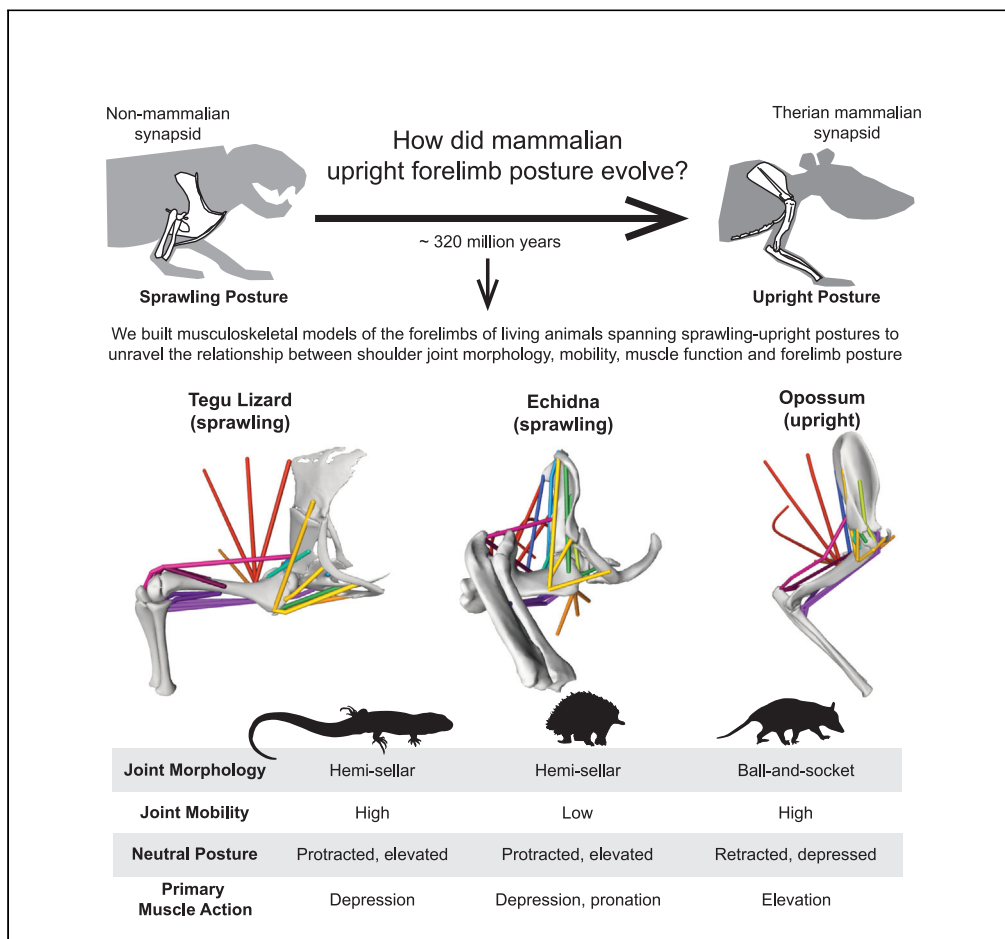## Article

Musculoskeletal modeling of sprawling and parasagittal forelimbs provides insight into synapsid postural transition

Robert J. Brocklehurst, Philip Fahn-Lai, Sophie Regnault, Stephanie E. Pierce

rbrocklehurst@fas.harvard.edu (R.J.B.)
spierce@oeb.harvard.edu (S.E.P.)

Highlights
Shoulder mobility and muscle leverage differ in sprawling vs. parasagittal tetrapods

Elevation leverage and joint versatility are key to therian parasagittal posture

Reptiles and monotremes both sprawl, but differ in aspects of shoulder function

Results give predictive power for the synapsid sprawling–parasagittal transition

Article

Musculoskeletal modeling of sprawling and parasagittal forelimbs provides insight into synapsid postural transition

Robert J. Brocklehurst,[1,4,*] Philip Fahn-Lai,[1,2] Sophie Regnault,[1,3] and Stephanie E. Pierce[1,*]

SUMMARY

The sprawling–parasagittal postural shift was a major transition during synapsid evolution, underpinned by reorganization of the forelimb, and considered key to mammalian ecological diversity. Determining when and how this transition occurred in the fossil record is challenging owing to limited comparative data on extant species. Here, we built forelimb musculoskeletal models of three extant taxa that bracket sprawling–parasagittal postures—tegu lizard, echidna, and opossum—and tested the relationship between three-dimensional joint mobility, muscle action, and posture. Results demonstrate clear functional variation between postural grades, with the parasagittal opossum occupying a distinct region of pose space characterized by a highly retracted and depressed shoulder joint that emphasizes versatility and humeral elevation. Applying our data to the fossil record support trends of an increasingly retracted humerus and greater elevation muscle moment arms indicative of more parasagittal postures throughout synapsid evolution.

INTRODUCTION

Extant therian mammals (marsupials and placentals) can be distinguished from other land-living quadrupeds by their derived parasagittal gait, with the limbs adducted close to the body midline and the limb joints aligned in a single plane (Bakker, 1971; Biewener, 1990; Fischer and Blickhan, 2006). This contrasts with the sprawling postures plesiomorphic for tetrapods—still typified by extant non-avian reptiles and amphibians—which are characterized by abducted limbs and multiaxial joints (Bakker, 1971; Blob and Biewener, 2001; Nyakatura et al., 2019). A postural shift from sprawling to parasagittal is heralded as a major transition during mammalian evolution and has been hypothesized to confer several adaptive advantages (Bakker, 1971; Kemp, 2005). As well as possessing distinctive limb postures, extant therians occupy a wide array of niches and the forelimbs have been exapted and transformed to serve diverse ecological functions (Polly, 2007). Both the parasagittal posture and increased functional disparity of therian forelimbs have been attributed to their distinct shoulder morphology: the shoulder girdle is reduced and mobile, the ventrally facing glenoid means the limbs project ventrally rather than laterally, and the "ball-and-socket" glenohumeral joint is hypothesized to permit a wider range of motion (Luo, 2015).

The parasagittal posture and functionally diverse forelimbs of therians contrast with the sprawled posture and functionally constrained forelimbs of their earliest ancestors among the non-mammalian synapsids (Lungmus and Angielczyk, 2019; Romer, 1922). Synapsids possess a good fossil record that documents the origins of key mammalian traits (Kemp, 2005), yet there remains considerable disagreement over when major functional changes in forelimb use and posture occurred during the evolution of mammals. Previous authors have proposed shifts from sprawled to "semi-sprawled" postures with the origin either of therapsids (Kemp, 2005; Romer, 1922) or cynodonts (Jenkins, 1971a), and the evolution of fully parasagittal postures on the mammalian stem (Kemp, 2005), at the base of crown mammals (Romer, 1922), or within stem therians (Jenkins, 1971a). This conflict is primarily due to differing functional interpretations of preserved skeletal anatomy and reconstructed soft-tissue (Jenkins, 1971a; Kemp, 2005; Lai et al., 2018; Romer, 1922), a problem exacerbated by limited biomechanical data from extant taxa, particularly on how bones and soft tissues interact to produce forelimb movement. Owing to the disparity in their forelimbs, parasagittal and sprawling taxa are often examined independently of one another, with few studies explicitly comparing sprawling vs. parasagittal locomotion within the same biomechanical framework (Fahn-Lai et al., 2020; Jenkins and Goslow, 1983). Therefore, we currently lack comparative functional

[1]Museum of Comparative Zoology and Department of Organismic and Evolutionary Biology, Harvard University, Cambridge, MA 01239, USA

[2]Concord Field Station and Department of Organismic and Evolutionary Biology, Harvard University, Bedford, MA01730, USA

[3]Institute of Biological, Environment & Rural Sciences, Aberystwyth University, Aberystwyth, CeredigionSY23 3DA, UK

[4]Lead contact

*Correspondence:
rbrocklehurst@fas.harvard.edu (R.J.B.),
spierce@oeb.harvard.edu (S.E.P.)

https://doi.org/10.1016/j.isci.2021.103578

Reference Pose | Neutral Pose | Musculoskeletal Model

Tegu
Ret. Prot.
Supn.
Pron.
Elev.
Dep.

Echidna

Opossum

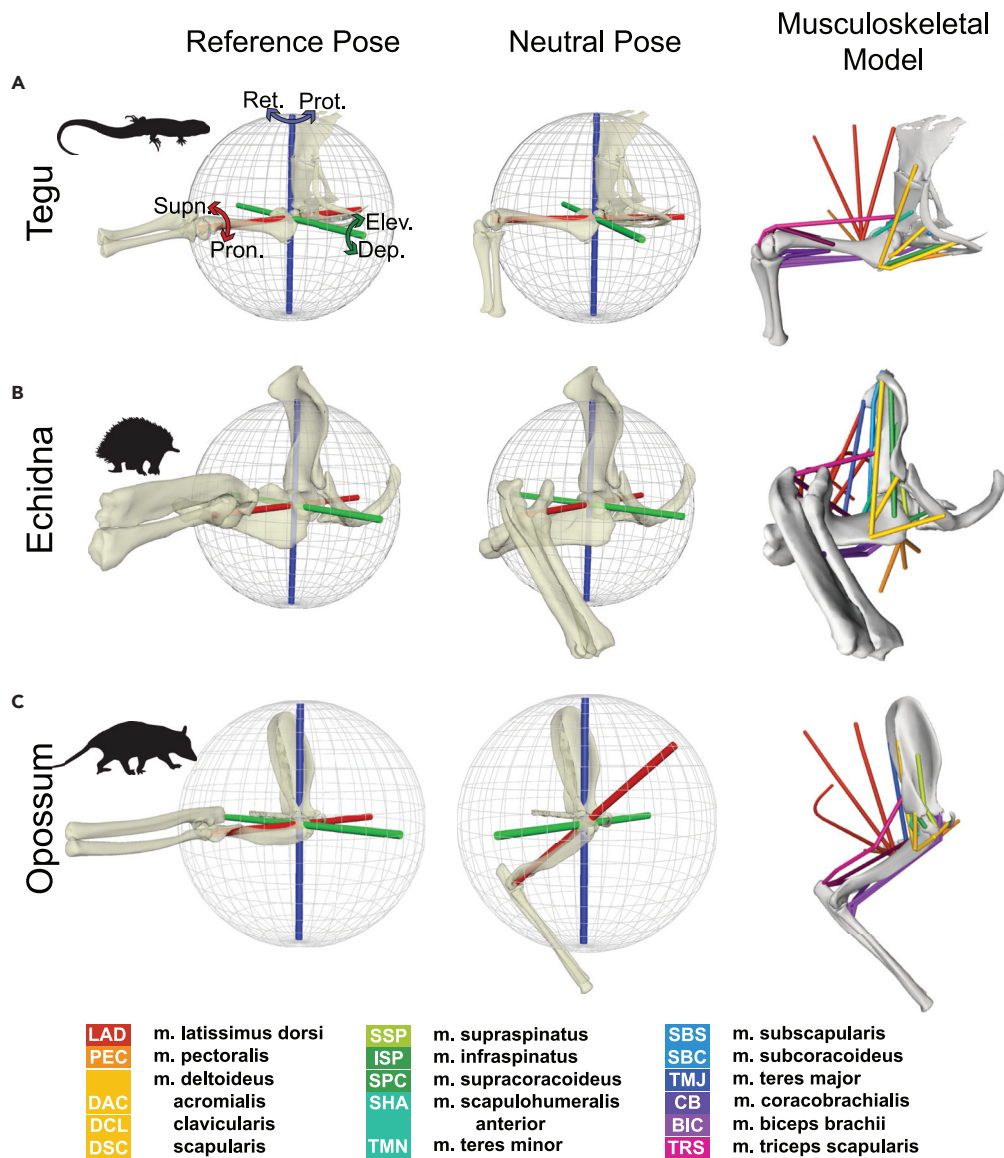| LAD | m. latissimus dorsi | SSP | m. supraspinatus | SBS | m. subscapularis |
PEC	m. pectoralis	ISP	m. infraspinatus	SBC	m. subcoracoideus
	m. deltoideus	SPC	m. supracoracoideus	TMJ	m. teres major
DAC	acromialis	SHA	m. scapulohumeralis	CB	m. coracobrachialis
DCL	clavicularis		anterior	BIC	m. biceps brachii
DSC	scapularis	TMN	m. teres minor	TRS	m. triceps scapularis

Figure 1. Musculoskeletal models of the forelimb across sprawling-parasagittal postures
Musculoskeletal models of the forelimb in the (A) tegu, (B) echidna, and (C) opossum. Left column: models in the global reference pose showing the joint coordinate system used to measure all joint angles. The blue Z-axes are (−) retraction and (+) protraction, the green Y-axes are (−) depression and (+) elevation, and red X-axes are long-axis rotation or (−) pronation and (+) supination. These axes are akin to changes in longitude, latitude, and heading on the joint sphere, respectively. Middle column: anatomically informed neutral poses, found by aligning the humeral head with the glenoid. Rotated joint axes show the movements on the joint sphere from the reference pose to neutral pose. Right column: OpenSim models, in the neutral pose, showing locations of the studied muscles with homologous muscles color coded as detailed in the legend.
See STAR Methods and Figures S1 and S2 for further details on model construction.

morphology data from extant taxa that may allow us to better interpret functional evolution along the mammalian stem lineage.

To address this data gap, we built forelimb musculoskeletal models of three extant taxa that functionally span sprawling and parasagittal postures (Figure 1): the Argentine black and white tegu (*Salvator meria-nae*), a representative squamate reptile with a classical sprawling gait, combining humeral long-axis rotation and limb retraction (flexion in a horizontal plane) (Jenkins and Goslow, 1983; Nyakatura et al., 2019); the short-beaked echidna (*Tachyglossus aculeatus*), a monotreme mammal with an "upright-sprawling" gait, in

which limb movement is primarily driven by humeral long-axis rotation (and rolling of the trunk) (Gambaryan and Kuznetsov, 2013; Jenkins, 1970; Regnault and Pierce, 2018); and the Virginia opossum (*Didelphis virginiana*), a therian mammal with a parasagittal gait, that mainly uses limb elevation (flexion in a dorsoventral plane) (Jenkins, 1971b; Jenkins and Weijs, 1979). Ecologically, the tegu and opossum have general terrestrial locomotor habits (Fahn-Lai et al., 2020; Jenkins, 1971b; Sheffield et al., 2011), whereas echidnas have a semi-fossorial lifestyle (Clemente et al., 2016). Although capable diggers, echidnas do this mainly for foraging; unlike truly fossorial mammals, they do not make complex burrows, and their primary means of locomotion is overground walking, not subterranean burrowing (Clemente et al., 2016). While all three taxa have previously served as model systems for understanding the evolution of posture in tetrapods (Butcher et al., 2011; Fahn-Lai et al., 2020; Regnault et al., 2020; Regnault and Pierce, 2018; Sheffield et al., 2011), opossums and echidnas have been used as extant comparators for fossil synapsids for decades (Jenkins, 1970, 1971b; Jenkins and Weijs, 1979; Lungmus and Angielczyk, 2021; Romer, 1922; Watson, 1917). While none of our taxa represent perfect analogs for what we see in the fossil record as they all possess their own apomorphic traits, they still provide useful information on the biomechanics of sprawling vs. parasagittal limb postures and the underlying functional consequences thereof.

At the glenohumeral joint, we measured three-dimensional osteological range of motion (ROM) and muscle moment arms (MMAs), two popular metrics among functional morphologists for comparing locomotor behavior across fossil taxa and their extant analogs or phylogenetic bracket (Brassey et al., 2017; Manafzadeh et al., 2021; Molnar et al., 2021; Otero et al., 2017). ROM data are commonly used to define the limits of possible poses that an animal might use in life, and have been used to reconstruct locomotor behavior in fossil species (Demuth et al., 2020; Manafzadeh and Padian, 2018; Nyakatura et al., 2015; Otero et al., 2017; Pierce et al., 2012). MMAs represent the leverage of muscles' around a joint and have been used to infer adaptations of the musculoskeletal system toward specific types of locomotor behaviors in extant and fossil taxa (Allen et al., 2021; Brassey et al., 2017; Maidment et al., 2014; Molnar et al., 2021; Regnault and Pierce, 2018). ROM-MMA analyses are typically performed using a "single axis" approach where mobility and muscle leverage are assessed about one axis of rotation at a time (Allen et al., 2021; Brassey et al., 2017; Molnar et al., 2021; Otero et al., 2017; Pierce et al., 2012; Regnault and Pierce, 2018). However, ROM in one degree of freedom can be influenced by rotations about other axes (Demuth et al., 2020; Manafzadeh and Padian, 2018; Regnault and Pierce, 2018) and MMAs covary with all rotational degrees of freedom, such that changing one angle at a time will produce different MMAs than changing multiple joint angles simultaneously (Hutchinson et al., 2015). As the sprawling–parasagittal postural transition involved major reorganization of the musculoskeletal system, and the shoulder joint has high mobility about all degrees of rotational freedom, understanding how joint and muscle function changed across the transition requires exploring ROM and MMAs within a 3D pose space.

Here, we explored broad-scale relationships between shoulder joint morphology, mobility, and muscle function across a large range of feasible limb poses and postures by modeling multiple degrees of freedom simultaneously (Manafzadeh and Padian, 2018). Based on previous studies of osteological ROM and interspecific differences in joint and limb morphology (Fahn-Lai et al., 2020; Jenkins, 1970, 1993; Luo, 2015; Regnault and Pierce, 2018), we predicted that shoulder joint ROM would be substantially greater in the opossum, with its ball-and-socket glenohumeral joint, than either the tegu or echidna which have hemi-sellar joints. We also predicted that MMAs about the glenohumeral joint would be highest in those specific degrees of freedom most important for locomotion based on *in vivo* data: long-axis rotation and retraction in the tegu, long-axis rotation in the echidna, and elevation in the opossum (Jenkins, 1970, 1971b; Jenkins and Goslow, 1983; Jenkins and Weijs, 1979; Regnault and Pierce, 2018). Validating these hypotheses using *in silico* musculoskeletal models is key to providing the methodological framework for interpreting posture and locomotion in fossils, for which experimental data are impossible to collect. Our results show that there is a complex relationship between posture, morphology, and joint and muscle function, but also reveal key similarities and differences between both sprawling and parasagittal taxa and between different types of sprawlers. We use these data, in combination with anatomical transformations preserved in the fossil record, to hypothesize when major shifts in shoulder joint function and forelimb posture occurred during synapsid evolution.

RESULTS

ROM analyses

Range of motion (ROM) at the glenohumeral joint was determined from an anatomical neutral pose, while joint angles were measured relative to a standard reference pose (Figure 1 and STAR Methods). ROM was
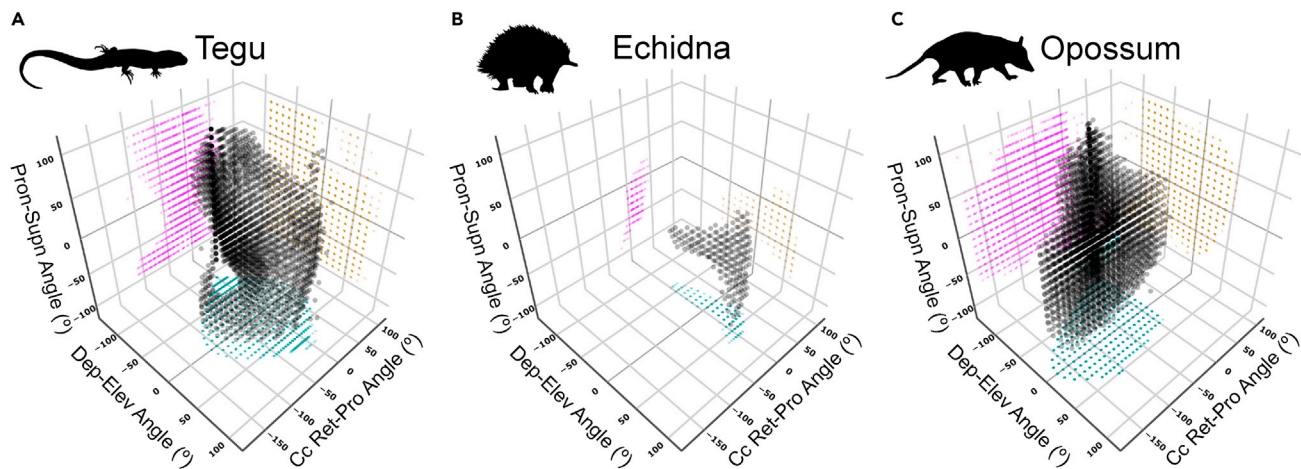
Figure 2. Glenohumeral joint range of motion (ROM) analysis

ROM envelopes for the glenohumeral joint in the (A) tegu, (B) echidna, and (C) opossum, where each point is a viable pose and its position in 3D pose space represents angles of rotation about the three joint axes. ROM envelopes are plotted in cosine-corrected (cc) Euler space to correct for distortion of distances between points as depression-elevation angles tend toward $\pm 90°$. Projected points are color coded according to the two axes of rotation which make up the plane (cyan on the ZY plane, magenta on the ZX plane, and gold on the XY plane). For interactive version of this plot see the Shiny web app in supplemental information (https://robert-brocklehurst.shinyapps.io/rom_mma_app/).

Abbreviations: Ret-Pro, Retraction-Protraction; Dep-Elev, Depression-Elevation; Pron-Supn, Pronation-Supination.

For more detailed views of the projected points, see Figure S4. For additional ROM sensitivity analyses in the echidna, see Figure S5.

simulated about multiple degrees of freedom simultaneously, using a modified version of existing code (Manafzadeh and Padian, 2018), and plotted as a 3D pose space where each graphical axis represents an angle of rotation about three orthogonal joint axes: retraction-protraction (Z-axis), depression-elevation (Y-axis), and supination-pronation (X-axis). Shoulder joint rotations were defined with respect to the reference pose: protraction brings the elbow cranially and retraction brings the elbow caudally in the horizontal plane; elevation brings the elbow dorsally and depression brings the elbow ventrally in the vertical plane; pronation internally rotates the humerus and supination externally rotates the humerus. Poses were deemed viable if there was no bony intersection between the humerus and scapulocoracoid, and if the humeral head remained in articulation with the glenoid (see STAR Methods and Figure S3).

Total glenohumeral joint ROM—measured as the volume of an alpha shape wrapped around all viable poses—was greatest in the opossum, followed closely by the tegu (alpha hull volumes 1,873,417 degrees^3 and 1,280,653 degrees^3, respectively), and both were orders of magnitude greater than the echidna (alpha hull volume 94,550 degrees^3). The echidna's ROM envelope is narrowest along the protraction-retraction axis and widest along the elevation-depression axis, meaning the humerus has the least mobility in the horizontal plane and greatest mobility in the vertical plane (Figure 2). This pattern of mobility is consistent with prior work on echidna osteological ROM (Regnault and Pierce, 2018). ROM in the tegu and the opossum is generally more evenly distributed in all three dimensions, although the shape of the tegu ROM envelope is more complex than that of the opossum, indicating greater interactions between degrees of freedom (Figures 2 and S4). The ROM envelopes of the tegu (and echidna) and opossum also occupy different regions within pose space, owing to differences in the neutral pose and underlying joint anatomy. While the tegu pose space is centered around the reference coordinate system, the sampled poses in the opossum occur at high retraction and depression angles, i.e., the humerus generally points more caudally and ventrally (Figures 2 and S4). This reflects differences in habitual limb posture (sprawled vs. parasagittal) and glenoid orientation (lateral vs. ventral) (Figure 1).

MMA analyses

Summed MMA: Global patterns

Muscle moment arms (MMAs) were estimated for all homologous muscles that cross the shoulder joint (Figure 1) and for each viable pose across the simulated pose space (Figure 2). To compare similarities and differences in overall muscle leverage across species, we summed size-normalized muscle moment arms at each pose for each degree of freedom (STAR Methods). Looking at the distributions of summed normalized
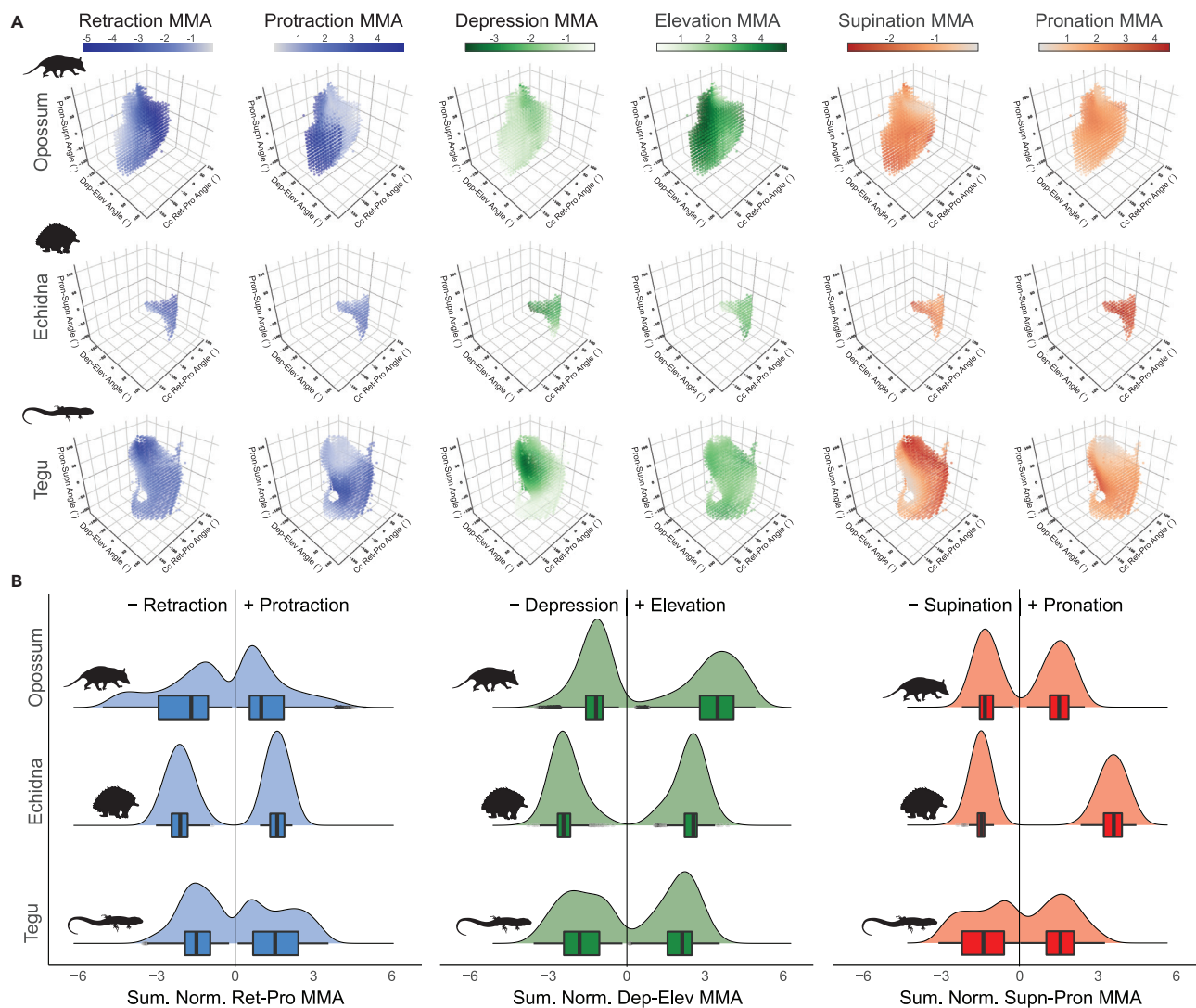
Figure 3. Glenohumeral joint summed muscle moment arm (MMA) analysis

Muscle moment arms (MMAs) across pose space in the tegu, echidna, and opossum. (A) Summed normalized MMAs at each glenohumeral joint pose; these plots are similar to the ones in Figure 2, but with points color coded according to MMAs for specific degrees of freedom. Color and opacity of the dots reflect size of the moment arms, with darker colors indicating larger moments arm and lighter colors indicating smaller moment arms. (B) Summary distribution and boxplots showing medians for the distributions of summed normalized muscle moment arms across pose space. These plots are "1D" representations of the data, showing the numerical distribution of summed MMA values, rather than their spatial distribution across pose space. For interactive version of panel (A) see Shiny web app in supplemental information (https://robert-brocklehurst.shinyapps.io/rom_mma_app/).

Abbreviations: cc, cosine-corrected; Ret-Pro, Retraction-Protraction; Dep-Elev, Depression-Elevation; Supn-Pron, Supination-Pronation.

MMAs across pose space for each species (Figure 3A) and their numerical summaries (Figure 3B), we see the highest median values for humeral retraction (pulling the elbow caudally) in the echidna (Figure 3B), but the highest peak values for retraction in the opossum (Figures 3A and 3B). These high retraction MMA values in the opossum occur when the humerus is protracted or at low retraction angles (>−50°) (Figure 3A). Median values for humeral protraction (pulling the elbow cranially) are greater in the tegu and echidna than in the opossum (Figure 3B), but the opossum and tegu have higher peak values. These peak values of protraction occur in the tegu either when the humerus is elevated and pronated or depressed and supinated (Figure 3A), and at extreme retraction angles in the opossum (Figure 3A).

For humeral depression (pulling the elbow ventrally), the opossum has the lowest median MMA values, and the echidna has the highest; however, peak values for depression are similar in the echidna and the tegu
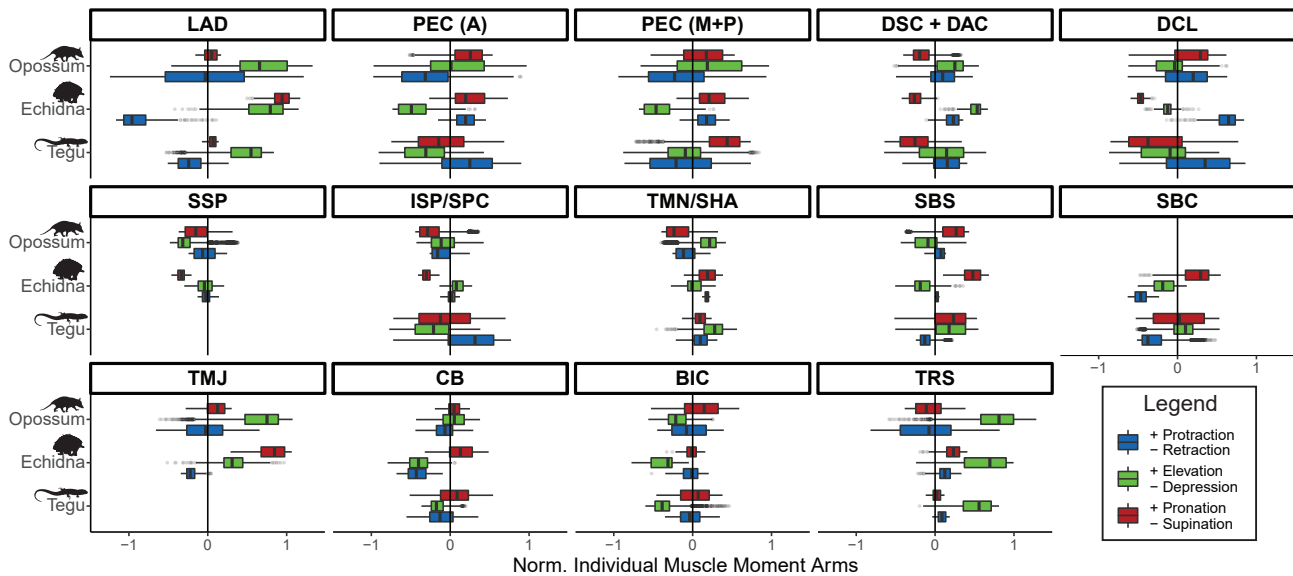
Figure 4. Glenohumeral joint muscle moment arm (MMA) analysis for individual muscles

Boxplots showing median values and distributions of normalized muscle moment arms (MMAs) for the different muscles modeled in the tegu, echidna, and opossum. Homologous muscles are indicated by a forward slash. Aggregated muscles are indicated by a plus. See Figure 1 for muscle name abbreviations. These plots are "1D" representations of the data, showing the numerical distribution of individual MMA values, rather than their spatial distribution across pose space. For interactive plots of individual muscle MMAs across pose space (similar to those in Figure 3A), see Shiny web app in supplemental information (https://robert-brocklehurst.shinyapps.io/rom_mma_app/). For additional comparisons of muscle function in the tegu vs. opossum, see Figure S6, and for the tegu vs. echidna, see Figure S7.

(Figure 3B). In both the tegu and echidna, humeral depression MMAs are greatest at more depressed joint angles (Figure 3). Peak and median MMA values for elevation (pulling the elbow dorsally) are lowest in the tegu, intermediate in the echidna, and greatest in the opossum (Figure 3B). The opossum has generally high values for summed elevation MMAs, but they are greatest at high retraction angles and with the humerus depressed below the horizontal (Figure 3A).

Both median and peak MMA values for humeral pronation (internal rotation of the humerus) are substantially higher in the echidna than in either the tegu or the opossum (Figure 3B), and they are distributed evenly across the echidna's pose space (Figure 3A). Emphasis on pronation MMAs in the echidna is consistent with prior work (Regnault and Pierce 2018). Median MMA values for supination (external rotation of the humerus) are greatest in the echidna but peak values are highest in the tegu (Figure 3B). These peak values occur when the tegu humerus is pronated (Figure 3A).

Individual MMA: muscle function

The observed similarities and differences in overall summed MMAs are the cumulative result of the actions of individual muscles (Figure 4, shiny app in supplemental information). To assess each muscles contribution, we looked at the summary distributions of each muscle's MMAs across pose space (Figure 4) and compared their actions between taxa. The extrinsic muscles are discussed first, and then the intrinsic muscles are discussed in order from proximal to distal. For the echidna, actions of individual muscles are in general agreement with those published previously (Regnault and Pierce, 2018).

In all three taxa studied, the m. latissimus dorsi (LAD) elevates and pronates the humerus, but whereas in the tegu and echidna this muscle strictly retracts, in the opossum it both protracts and retracts. M. latissimus dorsi retraction and pronation MMAs are particularly high in the echidna, and elevation MMAs are highest in the echidna and opossum. The function of the m. pectoralis (PEC) differs between taxa. In the opossum, both anterior (PEC A) and more posterior parts (PEC M + P) elevate, pronate, and retract the humerus, while in the echidna both parts serve to protract, depress, and pronate the humerus. The tegu possesses different MMAs in different parts of the muscle; anteriorly it supinates, depresses, and protracts the humerus, but posteriorly it pronates and retracts, with lower depression and greater elevation MMAs

(Figure 4). For the m. deltoideus, the acromial and scapular portions of this muscle (DAC + DSC) have similar functions in all three taxa, elevating, supinating, and protracting the humerus, whereas the clavicular portion (DCL) behaves differently; in the tegu and echidna it protracts and supinates the humerus, but in the opossum it pronates it.

The m. supraspinatus (SSP) is only present in the opossum and echidna and supinates and retracts in both, but also depresses in the opossum. The m. infraspinatus (ISP) of the opossum has MMAs for supination, depression, and retraction, but in the echidna this muscle elevates the humerus. The homologous muscle in the tegu, the m. supracoracoideus (SPC), also depresses the humerus, but protracts rather than retracts (Figure 4). The m. teres minor (TMN) of the opossum and echidna is homologous with the tegu m. scapulohumeralis anterior (SHA) (Fahn-Lai et al., 2020). In the tegu and opossum, this muscle acts to elevate the humerus but it elevates and depresses in the echidna. In the tegu and echidna, this muscle also pronates and protracts the humerus but has the opposite actions (retraction and supination) in the opossum.

The m. subcoracoideus (SBC) is only present in the tegu and echidna and acts to retract the humerus in both taxa, while also elevating in the tegu, but depressing and pronating in the echidna (Figure 4). The m. subscapularis (SBS) is present in all three taxa, and although it always has a pronating function, it behaves differently in the opossum and echidna vs the tegu; depressing and protracting the humerus in the two mammals but retracting and elevating it in the reptile. The m. teres major (TMJ) is present only in the opossum and echidna. It both retracts and protracts in the opossum, but only retracts in the echidna (Figure 4). In both taxa, this muscle elevates and pronates the humerus, but the echidna has larger pronation MMAs and the opossum has larger elevation MMAs (Figure 4). The m. coracobrachialis (CB) depresses the humerus in the echidna and tegu but depresses and elevates in the opossum. This muscle also has larger pronation MMAs in the tegu and echidna. The m. biceps brachii (BIC) has similar actions, depressing the humerus in all three taxa and pronating it in the tegu and opossum. The m. triceps scapularis (TRS) has high MMAs for humeral elevation in all three taxa. In the tegu and echidna, this muscle has protraction and pronation MMAs but supinates the humerus more in the opossum and has higher MMAs for both retraction and protraction (Figure 4).

Sensitivity analyses

Humeral morphology and ROM

The echidna had the lowest glenohumeral ROM of our three taxa, suggesting that ROM is being constrained by bony morphology. To investigate how osteology might constrain ROM in the echidna, we modified the echidna model in two ways and reran the ROM analysis: first, we removed the expanded proximal epiphyses from the humerus by virtually "slicing" them off; second, we scaled the whole humerus to 75% its width, thus narrowing both the epiphyses and elongated humeral head (Figure S5). While there was no difference between the ROM envelope volume and shape comparing the base model and the model with the epiphyses removed (alpha hull volume 94,550 degrees^3), the model with the narrowed humerus showed a 43% increase in overall ROM (alpha hull volume 135,486 degrees^3) (Figure S5). This increase in total ROM volume was the result of additional poses being achieved in all three anatomical planes — but particularly with addition of more protracted, elevated, and supinated poses — indicating that ROM in the echidna is constrained by the wide, high aspect ratio humeral head.

Monte Carlo simulations of MMAs

We tested whether the differences observed in overall patterns of MMAs across our three taxa are robust to potential model error through a Monte Carlo simulation procedure (Wiseman et al., 2021), by randomly increasing or decreasing MMA values of individual muscles up to ±20%. This range is based on error rates in previous studies which estimated MMAs in various ways (Brown et al., 2003; Cox et al., 2019). To evaluate the results of the Monte Carlo simulations, we looked at the distribution of median values of MMAs across pose space, across the different simulations, for different degrees of freedom (Figure 5). Even with the simulated confidence intervals, the most important comparisons outlined above still hold. Elevation MMAs are greatest in the opossum, pronation MMAs are greatest in the echidna, and depression MMAs are greater in the tegu and echidna than in the opossum. For other degrees of freedom, there is some overlap between the 95% confidence intervals. In protraction, there is overlap between the echidna and tegu, but both are higher than the opossum. There is some overlap between the opossum and echidna for retraction, and all the confidence intervals of all three taxa overlap for supination.
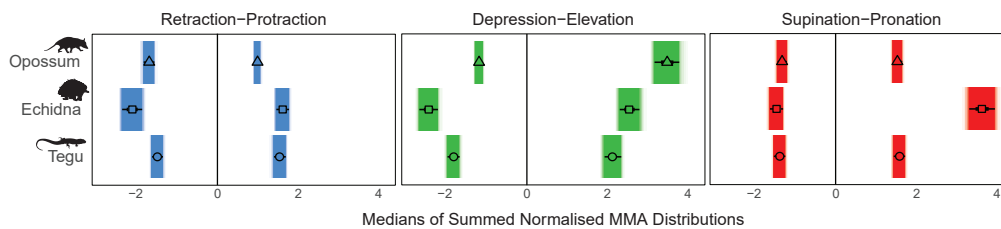
Figure 5. Monte Carlo sensitivity analysis
Median values for summed normalized muscle moment arms (MMAs) across pose space, with simulated 95% confidence intervals from the Monte Carlo sensitivity analysis. Point shapes indicate different taxa (triangle, opossum; square, echidna; circle, tegu). Bars are color-coded according to degree of freedom (retraction-protraction, blue; depression-elevation, green; supination-pronation, red). Retraction, depression, and supination are negative. Protraction, elevation, and pronation are positive.

Scapula motion and MMAs

Therian mammals, such as the opossum, have a mobile scapula and scapular motion contributes substantially to forelimb movements (Jenkins and Weijs, 1979). To account for this in our model, we systematically changed scapula pitch angle from horizontal to vertical (in 15° increments) and recalculated summed normalized MMAs. The pitch angles used correspond to changes in scapula orientation across stance phase (Jenkins and Weijs, 1979). We found that changes to scapula pitch angle predominantly affected moment arms for humeral elevation and depression, with minimal effect on retraction-protraction or supination-pronation MMAs. The sensitivity analysis shows that MMAs for elevation are highest when the scapula is at low angles to the horizontal and decrease as the scapula becomes more vertically oriented (Figure 6). However, across the whole range of scapula angles tested, the lowest values for elevation MMAs in the opossum are still greater than those seen in either the tegu or the echidna. We see the opposite pattern in depression MMAs — when the scapula is horizontally oriented these are lowest, and they increase in magnitude as scapula pitch angle increases. At high scapula pitch angles, the depression MMAs seen in the opossum approach the values observed in the tegu but are still lower than those of the echidna.

DISCUSSION

In this study, we used musculoskeletal modeling to investigate the functional differences in shoulder joint mobility and muscle action between sprawling and parasagittal forelimb postures. We used these models to explore 3D shoulder muscle moment arms (MMAs) across glenohumeral joint pose space, which is difficult to do experimentally, particularly at the shoulder joint with its high mobility in multiple degrees of freedom. We quantified similarities and differences in sprawling and parasagittal taxa and found important postural signatures in our data. Below, we discuss the key findings of our interspecific comparisons and use these data from extant taxa to interpret ROM, MMA, and postural evolution in the synapsid fossil record.

Therian ball-and-socket shoulder joint is not uniquely mobile

The mobile ball-and-socket shoulder (glenohumeral) joint of therian mammals has been suggested to underpin their extant ecological diversity, possessing a wide ROM envelope and allowing the forelimb to perform a greater range of movements and associated functions (Luo, 2015; Polly, 2007). Our results confirm that the shoulder joint in the opossum is indeed highly mobile as predicted, especially compared to its immediate sister taxon in this study, the sprawling monotreme echidna (Figure 2) (also see Jenkins, 1970; Regnault and Pierce, 2018). However, the tegu also had high total shoulder joint ROM, and both the opossum and tegu had considerably higher ROM (orders of magnitude) than the echidna (Figure 2). In particular, the tegu and opossum had much higher ranges of motion for humeral protraction-retraction and long-axis rotation than the echidna. This result indicates that the "hemi-sellar" glenoid joint morphologies of the tegu and echidna function differently, and that such joints are not inherently restrictive to motion (Jenkins, 1993). In fact, our sensitivity analyses indicate that humeral head shape may be a major constraint on shoulder joint ROM in the echidna (figure S5). While these conclusions are based on models which do not include translations, prior work has suggested that hemi-sellar joints may employ translation to achieve certain poses (Jenkins, 1993); future work including appropriate joint translations is thus predicted to increase ROM in the tegu and make the total mobility envelope volume of the tegu and opossum
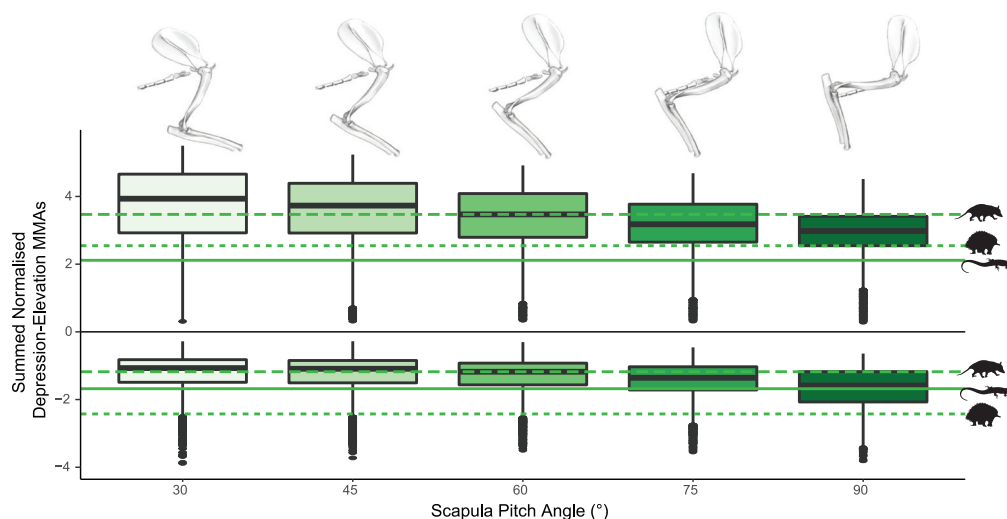
Figure 6. Opossum scapular orientation sensitivity analysis

Elevation-depression muscle moment arms (MMAs) across pose space in the opossum, at different scapula pitch angles. Boxplots show medians for summed normalized elevation (positive) and depression (negative) MMAs. The scapula was inclined 60° to the horizontal in the base opossum model. Horizontal lines are median values for elevation and depression MMAs in the different species from the base models.

more similar. Overall, when compared to more "classical" sprawling outgroups (e.g., lepidosaurs and crocodilians) with greater total ROM at the shoulder joint than monotremes (Baier and Gatesy, 2013; Molnar et al., 2021; Pierce et al., 2012), the high total mobility of the ball-and-socket shoulder joint in therians seems less extreme, and a less compelling explanation for therian forelimb diversity.

However, total ROM is not the only important metric when assessing joint mobility and function (Richards et al., 2021). For example, the shoulder joint ROM envelope of the opossum had a less complex shape than the tegu, suggesting reduced constraints on ROM via less interactions between different degrees of rotational freedom (Figure S4). The therian shoulder joint also operates in a fundamentally different region of pose space (Figure 2) — at generally higher retraction and depression angles (Jenkins, 1971b). Anatomically, this correlates with differences in glenoid orientation, which is ventral in parasagittal therians but lateral in sprawlers (Jenkins, 1971a; Luo, 2015). Functionally, this difference in limb orientation leads to differences in limb loading, with sprawled limbs loaded in bending and torsion, and parasagittal limbs loaded primarily in bending and compression (Biewener, 1990; Blob and Biewener, 1999, 2001). The adaptive significance of this remains unclear, but several hypotheses have been put forward. As long-bones of the fore- and hindlimbs are generally much more resistant to compression than to bending or torsional loads (Brassey et al., 2013), we would expect parasagittal taxa to experience lower limb bone stresses. It has also been suggested that, due to those lower stresses, parasagittal taxa might have evolved lower limb safety factors (Blob et al., 2014), and reduced the need for investing in heavy and metabolically expensive bone (Lanyon, 1991). Finally, animals with parasagittal postures require less muscular effort to support their body weight, as they transmit more of it directly through the limb bones; this results in lower energetic costs through reduced muscular effort and facilitates the evolution of larger body sizes by removing the constraints of requiring muscular support (Bakker, 1971).

Shoulder muscle elevation leverage key to parasagittal posture

Based on experimental studies of joint kinematics and muscle activation patterns (Jenkins, 1971b; Jenkins and Weijs, 1979), we predicted the opossum would have the greatest summed MMAs for humeral elevation. Note that under our standardized joint coordinate system that allows sprawling and parasagittal postures to be directly compared (Figure 1 and STAR Methods), humeral elevation at high retraction angles corresponds to the more traditional "flexion" in the parasagittal plane (Jenkins and Weijs, 1979). The opossum did indeed have the highest MMAs for humeral elevation out of the three taxa studied here (Figure 3), and this result was supported by our sensitivity analysis using Monte Carlo simulations (Figure 5).

Increased MMAs for forelimb elevation — particularly at high glenohumeral retraction angles — may therefore be an important part of the reorganization of the musculoskeletal system over the course of mammalian evolution.

The increased muscle leverage for elevation in the opossum is due to several factors. The m. teres major imparts a large elevation MMA (Figure 4) and contributes considerably to humerus elevation in mammals. Note that his muscle is absent in lepidosaurs, and although a m. teres major has been identified in crocodilians and turtles, its homology with the mammalian m. teres major is debated (Diogo et al., 2018; Molnar and Diogo, 2021). When comparing our two mammals, the m. teres major has larger elevation MMAs in the parasagittal opossum than in the sprawling echidna (Figure 4) indicating a postural effect. There are also several muscles that generally act as elevators in all three taxa but have greatest MMAs in the opossum (e.g., m. triceps scapularis), or which have different functions between taxa — acting as elevators in the opossum but depressors in the tegu and echidna (e.g., m. coracobrachialis, m. pectoralis) (Figure 4).

Of the muscles whose elevation-depression actions differ between taxa, the m. pectoralis is of key interest as the muscle appears to change its function across pose space. In both the tegu and opossum, which share large regions of pose space (Figure 2), the middle and posterior parts of the m. pectoralis showed a pattern whereby its MMA trends from depression to elevation with increasing humeral retraction angles (Figure S6; also see shiny app in supplemental information.). While the m. pectoralis is an important humeral retractor and antigravity "adductor" muscle in sprawling tetrapods (Allen et al., 2010; Regnault and Pierce, 2018), it helps drive locomotion via humeral elevation during the power stroke of stance in parasagittal therians (Jenkins and Weijs, 1979). Therefore, our results imply that during the sprawling–parasagittal transition, changes in muscle function may have come about purely through increasing humeral retraction angles via reorientation of the glenohumeral joint.

Elevation MMAs were also impacted by changes to the orientation of the scapula — with MMAs increasing as scapular pitch angle becomes more horizontal. As the measured changes in scapula pitch effectively correspond to different stages of stance phase (Jenkins, 1971b; Jenkins and Weijs, 1979), our results suggest that elevation MMAs are highest at the beginning of stance when the scapula is closest to the horizontal and decrease throughout the stance phase as the scapula becomes more vertical. Holding the humerus in its anatomical neutral pose and plotting glenohumeral elevation MMAs for individual muscles against changes in scapula pitch (Figure 7), we see changes in MMAs with increasing scapula angle also correspond to differences in muscle activation timing recorded by electromyography (Jenkins and Weijs, 1979). The m. pectoralis and caudal parts of the m. latissimus dorsi have higher elevation MMAs at lower (more horizontal) scapula angles and are active earlier in stance phase (Figure 7). On the other hand, the cranial part of the m. latissimus dorsi is active at the end of stance phase and has its highest elevation MMAs at high (near vertical) scapula angles (Figure 7). The mobile scapula is a therian innovation (Luo, 2015), and our models indicate that scapula motion has substantial effects on forelimb muscle action related to humerus elevation.

Echidna and tegu sprawl in different ways: spin vs. swing

The echidna and tegu are both classed as "sprawlers" based on their elevated (abducted) limbs and low humeral retraction angles (Jenkins, 1970, 1971b; Jenkins and Goslow, 1983). They shared some similarities in MMAs consistent with this, e.g., high MMAs for humeral depression (Figure 3). In sprawling animals, humeral depression corresponds to the adduction action of support musculature resisting abduction moments generated by laterally placed ground reaction forces (Blob and Biewener, 2001; Jenkins and Goslow, 1983). However, there were also several key differences between the echidna and tegu. The echidna had the greatest summed MMAs for humeral pronation (Figure 3) as expected, based on its reliance on humeral long-axis rotation during propulsion (Jenkins, 1970; Regnault and Pierce, 2018), a result supported by our Monte Carlo simulations (Figure 5). Many of the echidna's individual muscles possessed higher MMAs for pronation than their homologs in the tegu (Figure 4), but particularly the m. latissimus dorsi, which has a derived attachment site on the distal humeral entepicondyle (Regnault et al., 2020; Regnault and Pierce, 2018). The echidna also possesses muscles absent in the tegu; of these, the m. teres major has a substantial pronation MMA (Figure 4).

Contrary to our predictions, the tegu did not have greater MMAs than the echidna for humeral retraction (Figures 3 and 5), despite the prominent role of retraction in the classical sprawled gait (Jenkins and
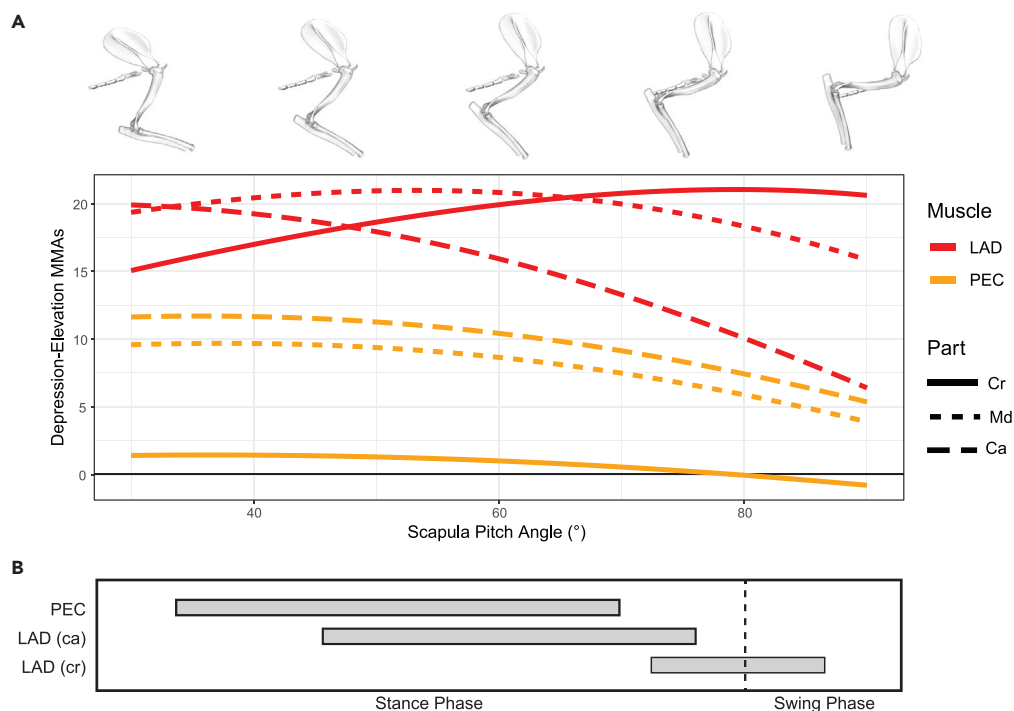
Figure 7. Changes in scapula angle, MMA, and muscle activation across "stance" in the opossum

(A) Raw, unscaled glenohumeral joint depression-elevation MMA values plotted against scapula pitch angle for the m. latissimus dorsi and m. pectoralis in the opossum. For this analysis, the glenohumeral joint was held in the anatomical neutral pose and only scapula pitch angle was changed.

(B) *In vivo* patterns of muscle activation for the m. pectoralis and m. latissimus dorsi during locomotion in the opossum, taken from Jenkins and Weijs (1979). Gray bars indicate when the muscle is active. Abbreviations: PEC, m. pectoralis; LAD, m. latissimus dorsi; cr, cranial; md, middle; ca, caudal.

Goslow, 1983; Nyakatura et al., 2019). In fact, the tegu had lower MMAs than the echidna in almost all degrees of freedom, both in the base model and in our Monte Carlo simulation (Figures 3 and 5). Although the echidna possesses extra muscles, many of the homologous muscles present in both taxa also have lower median MMAs in the tegu than the echidna (Figure 4). This is also true if we only compare poses which are viable in both taxa (Figure S7). Compared with the echidna, many muscles in the tegu insert more proximally on the humerus, and the humerus itself is much more gracile, with smaller epiphyses and a more rounded humeral head (Fahn-Lai et al., 2020; Regnault et al., 2020); this brings the muscle insertion sites closer to the axes of rotation, reducing MMAs but increasing the arc of the limb.

Given the difference in shoulder joint mobility between these two taxa (Figure 2), and the known trade-off between MMA and a muscle's working range for a given fiber length (Lieber and Fridén, 2001), we interpret these results in terms of balancing different aspects of forelimb function. Studies of forelimb muscle properties in both the echidna and tegu show that there is little specialization in terms of working range or force production, and generally the muscles have low architectural disparity (Fahn-Lai et al., 2020; Regnault et al., 2020). The tegu forelimb has generally lower MMAs and high shoulder joint ROM, which may represent adaptation for force production across a high muscle working range within the constraints of unspecialized muscles with average fiber lengths. On the other hand, the high MMA values seen in the echidna indicate adaptation for production of higher joint moments (particularly in pronation), presumably as an adaptation for scratch digging (Clemente et al., 2016), with the reduced muscle working range rendered moot by the restrictive nature of the glenohumeral joint.

The digging habits of echidnas have led to comparisons with fossorial therian mammals, in particular talpid moles (Sansalone et al., 2020), which have evolved a secondarily sprawling posture (Lin et al., 2019a). However, despite some superficial similarities in terms of humeral shape, e.g., the broadened epicondyles, the humeri of echidnas and talpids are morphologically and functionally distinct (Sansalone et al., 2020).
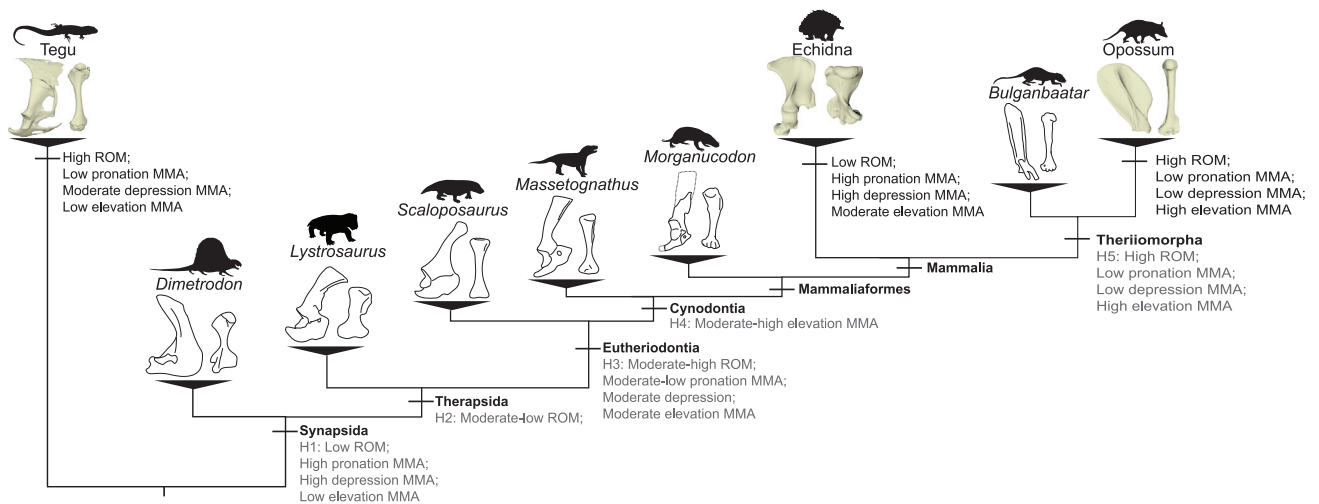
Figure 8. Evolution of synapsid shoulder joint and muscle function

Proposed changes in synapsid forelimb function, plotted across a simplified phylogeny, showing scapulae and humeri for representative taxa. Black annotations are results from the present study; gray annotations are hypothesized changes in forelimb ROM and MMAs based on anatomical transformations observed in fossil synapsids. Silhouettes illustrating *Massetognathus* and *Scaloposaurus* modified from artwork by Nobu Tamura. All other silhouettes are taken from phylopic.org. Silhouettes illustrating *Bulganbataar*, *Morganucodon*, and *Dimetrodon* are credited to Lucas Weaver (modified after artwork by MisakiOuchida), "FunkMonk" (Michael B. H.), and Dmitry Bogdanov, respectively.

Talpids possess the therian "ball-and-socket" glenoid, and *in vivo* XROMM data show that the talpid glenohumeral joint is much more mobile than the echidna's (Lin et al., 2019a, 2019b). Comparative analysis of shoulder joint muscle properties has also showed that the echidna is much more like a sprawling tegu lizard in terms of muscle architecture than it is to a fossorial talpid mole (Regnault et al., 2020). Therefore, while some aspects of forelimb functional morphology in the echidna likely reflect adaptations to digging, these adaptations have arisen in a specific morphological and evolutionary context, one which is very different from fossorial therian mammals.

Major functional shifts in synapsid forelimb evolution

Our biomechanical framework highlights several similarities and differences between the tegu, echidna, and opossum that can provide a powerful means to interpret postural shifts in the fossil record. Below, we use the results from our musculoskeletal models to predict how shoulder joint function may have changed across the sprawling–parasagittal transition in synapsids and put forward hypotheses on the evolution of joint and muscle function at major ancestral nodes along the mammalian stem. Our goal is to better understand the overall evolutionary trends in posture, not to assign particular postural grades ("sprawling","semi-sprawling", and "parasagittal") to any specific clade (Jenkins, 1971a; Kemp, 2005; Romer, 1922). Further, it is important to acknowledge that hypotheses of biomechanical similarity need not imply behavioral similarity, and that similar biomechanical functions can be employed by animals with distinct ecologies (Lauder, 1981; Lungmus and Angielczyk, 2021; Wainwright et al., 2005).

The most basal grade of fossil synapsids, the "pelycosaurs", is reconstructed with a sprawling posture based on joint and limb morphology. Within the forelimb, they possessed a craniocaudally elongated screw-shaped glenoid, which is proposed to greatly constrain the motion of the humerus and emphasize long-axis rotation (Romer, 1922; Jenkins, 1971a; Hopson, 2015). The humerus of "pelycosaurs" also featured a wide humeral head and expanded epiphyses for muscle attachment (Romer, 1922) (Figure 8). Although often compared to lepidosaurs owing to their more generalist terrestrial ecology (Hopson, 2015; Romer, 1922), "pelycosaurs" share important aspects of their forelimb functional morphology with the echidna: restricted glenohumeral ROM, emphasis on humeral long-axis rotation movements, wide humeral heads, and expanded epiphyses (Regnault and Pierce, 2018; Hopson, 2015; Lungmus and Angielczyk, 2021). Therefore, being reconstructed as sprawlers with an emphasis on humeral long-axis rotation, we might expect "pelycosaurs" to exhibit large MMAs for humeral pronation and depression (Figure 8), with the large epiphyses increasing moment arms of the m. pectoralis, which functions as a depressor and

pronator in extant sprawling taxa (Figure 4). As it is unlikely that "pelycosaurs" possessed an m. teres major (Molnar and Diogo, 2021), they most likely had low elevation MMAs, similar to the tegu.

With the origin of therapsids, the glenoid joint lost its craniocaudal screw-shape, instead becoming a dorsoventrally oriented notch (Kemp, 2005). However, most early branching and large bodied therapsids, including dinocephalians and anomodonts, retained laterally expanded proximal humeri with wide epiphyses and humeral heads (Lungmus and Angielczyk, 2019, 2021; Ray, 2006; Romer, 1922) (Figure 8). While ROM is predicted to be higher than in "pelycosaurs" because of changes to the glenoid joint, the wide humeral heads would still restrict ROM to some extent, as demonstrated in the echidna (Figure S5). In Eutheriodonta, which consists of more derived therapsids and non-mammalian cynodonts, there is a retention of the glenoid notch but a distinct shift toward more slender, gracile humeri (Jenkins, 1971a; Kemp, 1986; Lai et al., 2018; Lungmus and Angielczyk, 2019) (Figure 8). This combination of traits is hypothesized to increase shoulder joint mobility, particularly in protraction and retraction (Lai et al., 2018; Kemp, 1986), as demonstrated in the tegu (Figure 2). The glenoid also faced more caudally (Kemp, 1986; Lai et al., 2018), indicating the forelimbs may have operated at higher shoulder joint retraction angles. This in itself may have increased MMAs for elevation by changing the actions of certain muscles such as the m. pectoralis (Figures 4 and S6; also see shiny app in supplemental information.). There are also additional changes to the scapula and scapular musculature in cynodonts which would aid to increase elevation MMAs, e.g., the presence of a m. teres major evidenced by the laterally reflected axillary border of the scapula (Jenkins, 1971a; Lai et al., 2018; Romer, 1922). The more retracted humerus and increased elevation MMAs may suggest a trend to more parasagittal forelimb postures and function in this group (Jenkins, 1971a).

In mammaliaforms (and some early crown-group mammals), the glenoid maintains its hemi-sellar shape and caudolateral orientation (Luo, 2015). However, there does seem to be some diversity in the "openness" of the glenoid facet (Meng et al., 2017), and there is considerable variation in humeral shape (Lungmus and Angielczyk, 2021). Indeed, Mesozoic mammaliaforms explored several new niches not seen in non-mammalian cynodonts (Ji et al., 2006; Meng et al., 2017), additional evidence that forelimb-use and ROM is not necessarily inhibited by the possession of hemi-sellar joints or lack of a "typical" parasagittal posture. It is only in more crownward-theriomorph taxa that we see further morphological transformation of the shoulder joint, interpreted as indicative of more parasagittal posture (Luo, 2015; Sereno and McKenna, 1995) (Figure 8). Within stem therians, the glenoid reorients to face ventrally as opposed to laterally (Luo, 2015), in turn reorienting the humerus into a retracted and depressed neutral pose as seen in the opossum (Figure 1) and further changing the function of the shoulder musculature to favor elevation (Figure 3). The shape of the glenoid changes to the spheroidal "ball-and-socket" of modern therians (Luo, 2015), increasing glenohumeral ROM by removing constraints caused by interacting degrees of freedom (Figure S4), and there is evidence of a mobile shoulder girdle (Luo, 2015; Sereno and McKenna, 1995) that may have enhanced elevation of the limb as evidenced by our scapula pitch sensitivity analyses (Figure 6).

Conclusions

The origin of parasagittal posture and gait was a major event in the evolution of mammals, associated with fundamental reorganization of the musculoskeletal system, and expansion of forelimb functional disparity and ecological diversity. Here, we provide a biomechanical framework to quantify how sprawling and parasagittal forelimb postures and morphologies affect glenohumeral joint mobility, muscle function, and ultimately potential forelimb-use. Our data show that the parasagittal opossum had the highest shoulder joint ROM, consistent with its ball-and-socket joint morphology. However, the sprawling tegu also had high ROM, substantially higher than the echidna, and when combined with our sensitivity analyses, indicates that bony glenoid morphology is not the sole determinant of shoulder mobility. The opossum did have a less complex ROM envelope, suggesting a more versatile shoulder joint, with fewer constraints on motion owing to fewer interactions between degrees of freedom. The opossum shoulder joint also operated in a different region of pose space, with more retracted and depressed shoulder joint angles. Furthermore, our MMA results reveal important differences in muscle function both between and within postural grades. Our sprawling taxa emphasized humeral depression MMAs, which are necessary to resist the elevating (abducting) moments generated by the more horizontally directed ground reaction forces. This contrasted with the opossum, in which humeral elevation MMAs are emphasized. At the high shoulder retraction angles observed in the opossum, elevation acts to produce "flexion" in the parasagittal plane — the characteristic movement of therian locomotion. Therefore, a shoulder joint that functions at high retraction angles and

with high elevation MMAs likely represents an important indicator of parasagittal posture and gait. There were also obvious differences between our sprawlers; the echidna strongly emphasizes pronation, while the tegu has smaller and more equal distribution of MMA in multiple degrees of freedom. This dataset gives us the unique opportunity to better conceptualize musculoskeletal function across sprawling–parasagittal postures and can ultimately be used to test hypotheses we put forward on limb morphofunctional transformation in the synapsid fossil record.

Limitations of the study

As the musculoskeletal models used in this study require detailed anatomical information and are complex to build and analyze, we focused on a few exemplar taxa. Therefore, we do not sample the full range of morphological or functional variation present in extant tetrapods. While our models' ROM and MMA outputs have not been specifically validated against experimental data (although see Regnault et al., 2021), our model outputs do agree with previously published observations on locomotion in the literature (Jenkins, 1970; Jenkins and Goslow, 1983; Jenkins and Weijs, 1979; Nyakatura et al., 2019). In addition, our study is comparative in nature, and so, the values need not exactly match those from experimental data to achieve the study's goals (Bishop et al., 2021).

STAR★METHODS

Detailed methods are provided in the online version of this paper and include the following:

- KEY RESOURCES TABLE
- RESOURCE AVAILABILITY
  - Lead contact
  - Materials availability
  - Data and code availability
- EXPERIMENTAL MODEL AND SUBJECT DETAILS
  - Animals
- METHOD DETAILS
  - Shoulder musculoskeletal geometry
  - Model assembly
- QUANTIFICATION AND STATISTICAL ANALYSIS
  - Estimating and analyzing range of motion (ROM)
  - Estimating and analyzing muscle moment arms (MMA)
  - ROM and MMAsensitivity analyses
- ADDITIONAL RESOURCES

SUPPLEMENTAL INFORMATION

Supplemental information can be found online at https://doi.org/10.1016/j.isci.2021.103578.

AUTHOR CONTRIBUTIONS

R.J.B. and S.E.P. conceived and designed the study. P.F-L. and S.R. collected the original muscle data. R.J.B. built and analyzed the musculoskeletal models. R.J.B. and S.E.P. interpreted the results and drafted the manuscript. All authors edited the manuscript and gave final approval for publication.

DECLARATION OF INTERESTS

We declare we have no competing interests.

REFERENCES

Allen, V., Elsey, R.M., Jones, N., Wright, J., and Hutchinson, J.R. (2010). Functional specialization and ontogenetic scaling of limb anatomy in *Alligator mississippiensis*. J. Anat. *216*, 423–445. https://doi.org/10.1111/j.1469-7580.2009.01202.x.

Allen, V.R., Kilbourne, B.M., and Hutchinson, J.R. (2021). The evolution of pelvic limb muscle moment arms in bird-line archosaurs. Sci. Adv. *7*, eabe2778. https://doi.org/10.1126/sciadv.abe2778.

Baier, D.B., and Gatesy, S.M. (2013). Three-dimensional skeletal kinematics of the shoulder girdle and forelimb in walking *Alligator*. J. Anat. *223*, 462–473. https://doi.org/10.1111/joa.12102.

Bakker, R.T. (1971). Dinosaur physiology and the origin of mammals. Evolution *25*, 636–658. https://doi.org/10.2307/2406945.

Biewener, A.A. (1990). Biomechanics of mammalian terrestrial locomotion. Science *250*, 1097–1103.

Bishop, P.J., Falisse, A., De Groote, F., and Hutchinson, J.R. (2021). Predictive simulations of musculoskeletal function and jumping performance in a generalized bird. Integr. Org. Biol. *3*, obab006. https://doi.org/10.1093/iob/obab006.

Blob, R.W., and Biewener, A.A. (2001). Mechanics of limb bone loading during terrestrial locomotion in the green iguana (*Iguana iguana*) and American alligator (*Alligator mississippiensis*). J. Exp. Biol. *204*, 1099–1122.

Blob, R.W., and Biewener, A.A. (1999). In vivo locomotor strain in the hindlimb bones of *Alligator mississippiensis* and *Iguana iguana*: implications for the evolution of limb bone safety factor and non-sprawling limb posture. J. Exp. Biol. *202*, 1023–1046.

Blob, R.W., Espinoza, N.R., Butcher, M.T., Lee, A.H., D'Amico, A.R., Baig, F., and Sheffield, K.M. (2014). Diversity of limb-bone safety factors for locomotion in terrestrial vertebrates: evolution and mixed chains. Integr. Comp. Biol. *54*, 1058–1071. https://doi.org/10.1093/icb/icu032.

Brassey, C.A., Maidment, S.C.R., and Barrett, P.M. (2017). Muscle moment arm analyses applied to vertebrate paleontology: a case study using *Stegosaurus stenops* Marsh, 1887. J. Vertebr. Paleontol. *37*, e1361432. https://doi.org/10.1080/02724634.2017.1361432.

Brassey, C.A., Margetts, L., Kitchener, A.C., Withers, P.J., Manning, P.L., and Sellers, W.I. (2013). Finite element modelling versus classic beam theory: comparing methods for stress estimation in a morphologically diverse sample of vertebrate long bones. J. R. Soc. Interf. *10*, 20120823. https://doi.org/10.1098/rsif.2012.0823.

Brown, N.A., Pandy, M.G., Buford, W.L., Kawcak, C.E., and McIlwraith, C.W. (2003). Moment arms about the carpal and metacarpophalangeal joints for flexor and extensor muscles in equine forelimbs. Am. J. Vet. Res. *64*, 351–357. https://doi.org/10.2460/ajvr.2003.64.351.

Butcher, M.T., White, B.J., Hudzik, N.B., Gosnell, W.C., Parrish, J.H., and Blob, R.W. (2011). In vivo strains in the femur of the Virginia opossum (*Didelphis virginiana*) during terrestrial locomotion: testing hypotheses of evolutionary shifts in mammalian bone loading and design. J. Exp. Biol. *214*, 2631–2640. https://doi.org/10.1242/jeb.049544.

Clemente, C.J., Cooper, C.E., Withers, P.C., Freakley, C., Singh, S., and Terrill, P. (2016). The private life of echidnas: using accelerometry and GPS to examine field biomechanics and assess the ecological impact of a widespread, semi-fossorial monotreme. J. Exp. Biol. *219*, 3271–3283. https://doi.org/10.1242/jeb.143867.

Cox, S.M., Easton, K.L., Lear, M.C., Marsh, R.L., Delp, S.L., and Rubenson, J. (2019). The interaction of compliance and activation on the force-length operating range and force generating capacity of skeletal muscle: a computational study using a Guinea fowl musculoskeletal model. Integr. Org. Biol. *1*, obz022.

Delp, S.L., Anderson, F.C., Arnold, A.S., Loan, P., Habib, A., John, C.T., Guendelman, E., and Thelen, D.G. (2007). OpenSim: open-source software to create and analyze dynamic simulations of movement. IEEE Trans. Biomed. Eng. *54*, 1940–1950.

Demuth, O.E., Rayfield, E.J., and Hutchinson, J.R. (2020). 3D hindlimb joint mobility of the stem-archosaur *Euparkeria capensis* with implications for postural evolution within Archosauria. Sci. Rep. *10*, 15357. https://doi.org/10.1038/s41598-020-70175-y.

Diogo, R., Ziermann, J.M., Molnar, J., Siomava, N., and Abdala, V. (2018). Muscles of Chordates: Development, Homologies, and Evolution, First edition. (Routledge). https://doi.org/10.1201/b22498.

Fahn-Lai, P., Biewener, A.A., and Pierce, S.E. (2020). Broad similarities in shoulder muscle architecture and organization across two amniotes: implications for reconstructing non-mammalian synapsids. Peer *8*, e8556. https://doi.org/10.7717/peerj.8556.

Fischer, M.S., and Blickhan, R. (2006). The tri-segmented limbs of therian mammals: kinematics, dynamics, and self-stabilization—a review. J. Exp. Zool A. Comp. Exp. Biol. *305*, 935–952. https://doi.org/10.1002/jez.a.333.

Gambaryan, P.P., and Kuznetsov, A.N. (2013). An evolutionary perspective on the walking gait of the long-beaked echidna. J. Zool. *290*, 58–67. https://doi.org/10.1111/jzo.12014.

Hopson, J.A. (2015). Fossils, trackways, and transitions in locomotion. In Great Transformations in Vertebrate Evolution, K.P. Dial, N.H. Shubin, and E.L. Brainerd, eds. (IL: University of Chicago Press Chicago), pp. 125–141.

Hutchinson, J.R., Rankin, J.W., Rubenson, J., Rosenbluth, K.H., Siston, R.A., and Delp, S.L. (2015). Musculoskeletal modelling of an ostrich (*Struthio camelus*) pelvic limb: influence of limb orientation on muscular capacity during locomotion. PeerJ *3*, e1001.

Jenkins, F.A. (1993). The evolution of the avian shoulder joint. Am. J. Sci. *293*, 253–267. https://doi.org/10.2475/ajs.293.A.253.

Jenkins, F.A. (1971a). The postcranial skeleton of African cynodonts. Bull. Peabody Mus. Nat. Hist. *36*, 1–216.

Jenkins, F.A. (1971b). Limb posture and locomotion in the Virginia opossum (*Didelphis marsupialis*) and in other non-cursorial mammals. J. Zoolog. *165*, 303–315. https://doi.org/10.1111/j.1469-7998.1971.tb02189.x.

Jenkins, F.A. (1970). Limb movements in a monotreme (*Tachyglossus aculeatus*): a cineradiographic analysis. Science *168*, 1473–1475.

Jenkins, F.A., and Goslow, G.E. (1983). The functional anatomy of the shoulder of the savannah monitor lizard (*Varanus exanthematicus*). J. Morphol. *175*, 195–216. https://doi.org/10.1002/jmor.1051750207.

Jenkins, F.A., and Weijs, W.A. (1979). The functional anatomy of the shoulder in the Virginia opossum (*Didelphis virginiana*). J. Zoolog. *188*, 379–410. https://doi.org/10.1111/j.1469-7998.1979.tb03423.x.

Ji, Q., Luo, Z.X., Yuan, C.X., and Tabrum, A.R. (2006). A swimming mammaliaform from the Middle Jurassic and ecomorphological diversification of early mammals. Science *311*, 1123–1127.

Kambic, R.E., Roberts, T.J., and Gatesy, S.M. (2014). Long-axis rotation: a missing degree of freedom in avian bipedal locomotion. J. Exp. Biol. *217*, 2770–2782. https://doi.org/10.1242/jeb.101428.

Kemp, T.S. (2005). The Origin and Evolution of Mammals (Oxford University Press).

Kemp, T.S. (1986). The skeleton of a baurioidtherocephalian therapsid from the Lower Triassic (Lystrosaurus Zone) of South Africa. J. Vertebr. Paleontol. *6*, 215–232. https://doi.org/10.1080/02724634.1986.10011617.

Lai, P.H., Biewener, A.A., and Pierce, S.E. (2018). Three-dimensional mobility and muscle attachments in the pectoral limb of the Triassic cynodont *Massetognathus pascuali* (Romer, 1967). J. Anat. *232*, 383–406. https://doi.org/10.1111/joa.12766.

Lanyon, L.E. (1991). In Biomechanical Properties of Bone and Response of Bone to Mechanical Stimuli: Functional Strain as a Controlling Influence on Bone Modeling and Remodeling Behavior, B.K. Hall, ed. Bone (CRC Press), pp. 79–108.

Lauder, G.V. (1981). Form and function: structural analysis in evolutionary morphology. Paleobiology *7*, 430–442. https://doi.org/10.1017/S0094837300025495.

Lieber, R.L., and Fridén, J. (2001). Clinical significance of skeletal muscle architecture. Clin.Orthop.Relat. Res. *383*, 140–151.

Lin, Y.F., Konow, N., and Dumont, E.R. (2019a). How moles walk; it's all thumbs. Biol. Lett. *15*, 20190503. https://doi.org/10.1098/rsbl.2019.0503.

Lin, Y.F., Konow, N., and Dumont, E.R. (2019b). How moles destroy your lawn: the forelimb kinematics of eastern moles in loose and compact substrates. J. Exp. Biol. *222*. https://doi.org/10.1242/jeb.182436.

Lungmus, J.K., and Angielczyk, K.D. (2021). Phylogeny, function and ecology in the deep evolutionary history of the mammalian forelimb. Proc. R. Soc. B Biol. Sci. *288*. 2021.0494, 20210494. https://doi.org/10.1098/rspb.2021.0494.

Lungmus, J.K., and Angielczyk, K.D. (2019). Antiquity of forelimb ecomorphological diversity in the mammalian stem lineage (Synapsida). Proc. Natl. Acad. Sci. U S A. *116*, 6903–6907.

Luo, X. (2015). Origin of the mammalian shoulder. In Great Transformations in Vertebrate Evolution, K.P. Dial, N.H. Shubin, and E.L. Brainerd, eds. (University of Chicago Press), pp. 167–187.

Maidment, S.C., Bates, K.T., Falkingham, P.L., VanBuren, C., Arbour, V., and Barrett, P.M. (2014). Locomotion in ornithischian dinosaurs: an assessment using three-dimensional computational modelling. Biol. Rev. Camb Philos. Soc. *89*, 588–617. https://doi.org/10.1111/brv.12071.

Manafzadeh, A.R., and Gatesy, S.M. (2021). Paleobiological reconstructions of articular function require all six degrees of freedom. J. Anat. N/a. https://doi.org/10.1111/joa.13513.

Manafzadeh, A.R., and Gatesy, S.M. (2020). A coordinate-system-independent method for comparing joint rotational mobilities. J. Exp. Biol. *223*. https://doi.org/10.1242/jeb.227108.

Manafzadeh, A.R., Kambic, R.E., and Gatesy, S.M. (2021). A new role for joint mobility in reconstructing vertebrate locomotor evolution. Proc. Natl. Acad. Sci. U S A. *118*. https://doi.org/10.1073/pnas.2023513118.

Manafzadeh, A.R., and Padian, K. (2018). ROM mapping of ligamentous constraints on avian hip mobility: implications for extinct ornithodirans. Proc. Biol. Sci. *285*, 20180727. https://doi.org/10.1098/rspb.2018.0727.

Meng, Q.J., Grossnickle, D.M., Liu, D., Zhang, Y.G., Neander, A.I., Ji, Q., and Luo, Z.X. (2017). New gliding mammaliaforms from the Jurassic. Nature *548*, 291–296. https://doi.org/10.1038/nature23476.

Molnar, J.L., and Diogo, R. (2021). Evolution, homology, and development of tetrapod limb muscles. Diversity *13*, 393. https://doi.org/10.3390/d13080393.

Molnar, J.L., Hutchinson, J.R., Diogo, R., Clack, J.A., and Pierce, S.E. (2021). Evolution of forelimb musculoskeletal function across the fish-to-tetrapod transition. Sci. Adv. *7*, eabd7457. https://doi.org/10.1126/sciadv.abd7457.

Nyakatura, J.A., Allen, V.R., Lauströer, J., Andikfar, A., Danczak, M., Ullrich, H.J., Hufenbach, W., Martens, T., and Fischer, M.S. (2015). A three-dimensional skeletal reconstruction of the stem amniote *Orobates pabsti* (Diadectidae): analyses of body mass,centre of mass position, and joint mobility. PLoS One *10*, e0137284. https://doi.org/10.1371/journal.pone.0137284.

Nyakatura, J.A., Melo, K., Horvat, T., Karakasiliotis, K., Allen, V.R., Andikfar, A., Andrada, E., Arnold, P., Lauströer, J., Hutchinson, J.R., et al. (2019). Reverse-engineering the locomotion of a stem amniote. Nature *565*, 351–355. https://doi.org/10.1038/s41586-018-0851-2.

Otero, A., Allen, V., Pol, D., and Hutchinson, J.R. (2017). Forelimb muscle and joint actions in Archosauria: insights from *Crocodylus johnstoni* (Pseudosuchia) and *Mussaurus patagonicus* (Sauropodomorpha). PeerJ. *5*, e3976. https://doi.org/10.7717/peerj.3976.

Pierce, S.E., Clack, J.A., and Hutchinson, J.R. (2012). Three-dimensional limb joint mobility in the early tetrapod *Ichthyostega*. Nature *486*, 523–526. https://doi.org/10.1038/nature11124.

Polly, P.D. (2007). Limbs in mammalian evolution. In Fins into Limbs: Evolution, Development and Transformation, B.K. Hall, ed. (University of Chicago Press), pp. 245–268.

Pridmore, P.A. (1985). Terrestrial locomotion in monotremes (Mammalia: Monotremata). J. Zool. *205*, 53–73. https://doi.org/10.1111/j.1469-7998.1985.tb05613.x.

Ray, S. (2006). Functional and evolutionary aspects of the postcranial anatomy of Dicynodonts (synapsida, Therapsida).

Palaeontology *49*, 1263–1286. https://doi.org/10.1111/j.1475-4983.2006.00597.x.

Regnault, S., Fahn-Lai, P., Norris, R.M., and Pierce, S.E. (2020). Shoulder muscle architecture in the echidna (Monotremata: *Tachyglossus aculeatus*) indicates conserved functional properties. J. Mammal Evol. *27*, 591–603. https://doi.org/10.1007/s10914-020-09498-6.

Regnault, S., Fahn-Lai, P., and Pierce, S.E. (2021). Validation of an echidna forelimb musculoskeletal model using XROMM and diceCT. Front Bioeng Biotechnol *9*, 751518. https://doi.org/10.3389/fbioe.2021.751518.

Regnault, S., and Pierce, S.E. (2018). Pectoral girdle and forelimb musculoskeletal function in the echidna (*Tachyglossus aculeatus*): insights into mammalian locomotor evolution. R. Soc. Open Sci. *5*, 181400.

Richards, H.L., Bishop, P.J., Hocking, D.P., Adams, J.W., and Evans, A.R. (2021). Low elbow mobility indicates unique forelimb posture and function in a giant extinct marsupial. J. Anat. *238*, 1425–1441. https://doi.org/10.1111/joa.13389.

Romer, A.S. (1922). The locomotor apparatus of certain primitive and mammal-like reptiles. Bull. Am. Mus. Nat. Hist. *46*, 517–606.

Sansalone, G., Castiglione, S., Raia, P., Archer, M., Dickson, B., Hand, S., Piras, P., Profico, A., and Wroe, S. (2020). Decoupling functional and morphological convergence, the study case of fossorial mammalia. Front. Earth Sci. *8*. https://doi.org/10.3389/feart.2020.00112.

Sereno, P.C., and McKenna, M.C. (1995). Cretaceous multituberculate skeleton and the early evolution of the mammalian shoulder girdle. Nature *377*, 144–147. https://doi.org/10.1038/377144a0.

Sheffield, K.M., Butcher, M.T., Shugart, S.K., Gander, J.C., and Blob, R.W. (2011). Locomotor loading mechanics in the hindlimbs of tegu lizards (*Tupinambis merianae*): comparative and evolutionary implications. J. Exp. Biol. *214*, 2616–2630. https://doi.org/10.1242/jeb.048801.

Wainwright, P.C., Alfaro, M.E., Bolnick, D.I., and Hulsey, C.D. (2005). Many-to-one mapping of form to function: a general principle in organismal design? Integr. Comp. Biol. *45*, 256–262.

Watson, D.M. (1917). The evolution of the tetrapod shoulder girdle and fore-limb. J. Anat. *52*, 1–63.

Wiseman, A.L.A., Bishop, P.J., Demuth, O.E., Cuff, A.R., Michel, K.B., and Hutchinson, J.R. (2021). Musculoskeletal modelling of the Nile crocodile (*Crocodylus niloticus*) hindlimb: effects of limb posture on leverage during terrestrial locomotion. J. Anat. https://doi.org/10.1111/joa.13431.

STAR★METHODS

KEY RESOURCES TABLE

REAGENT or RESOURCE	SOURCE	IDENTIFIER
Biological samples		
Salvator merianae	United States Geological Survey Daniel Beard Center	SEP74
Tachyglossus aculeatus	University of Adelaide	SEP42
Didelphis virginiana	Massachusetts Division of Fisheries and Wildlife	SEP87
Deposited data		
Raw data including range of motion data, muscle moment arm data, and musculoskeletal models.	Harvard Dataverse https://dataverse.harvard.edu/	https://doi.org/10.7910/DVN/5CY3IC
Software and algorithms		
Meshmixer	Autodesk https://www.meshmixer.com/	Autodesk Meshmixer 2017
Maya	Autodesk https://www.autodesk.com/products/maya	Autodesk Maya 2019
OpenSim	https://simtk.org/projects/opensim	OpenSim Version 4.1
R	R Core Team https://www.r-project.org/	R Version 3.6.3
RStudio	RStudio Team https://www.rstudio.com/	RStudio Version 1.2.5033

RESOURCE AVAILABILITY

Lead contact

Further questions should be directed to the lead contact, Robert J. Brocklehurst (rbrocklehurst@fas.harvard.edu).

Materials availability

This study did not generate new reagents.

Data and code availability

- OpenSim models, as well as MMA and ROM results files for all three taxa and a local copy of the R Shiny visualization app are available to download through Harvard Dataverse: https://doi.org/10.7910/DVN/5CY3IC.

- No novel code was used in this study.

- Any additional information required to reanalyze the data reported in this paper is available from the lead contact upon request.

EXPERIMENTAL MODEL AND SUBJECT DETAILS

Animals

All specimens used here were obtained as cadavers from the source organizations listed in the key resources table. Specimens were used for dissection and contrast-enhanced CT scanning in previously published studies (Fahn-Lai et al., 2020; Regnault et al., 2020; Regnault and Pierce, 2018). Current lab accession numbers are listed in the key resources table, and further specimen details are available in Table S1.

METHOD DETAILS

Shoulder musculoskeletal geometry

All specimens used here were digitized as part of previous studies (Fahn-Lai et al., 2020; Regnault et al., 2020; Regnault and Pierce, 2018). Briefly, specimens were contrast-stained with Lugol's iodine and micro-CT scanned (for staining and scanning parameters, see Table S1) to capture both hard- and soft-tissue anatomy. Tomographic images were segmented using Mimics version 19 (Materialise NV, Leuven, Belgium) to extract musculoskeletal geometry. Muscle insertion and origin sites were painted onto the

forelimb bones in Mudbox (versions 2019, 2020, Autodesk Inc., San Rafael, CA, USA) and extracted as individual meshes. To facilitate creation and alignment of anatomical and joint coordinate systems (Kambic et al., 2014), geometric primitives – planes, spheres, cylinders – and convex hulls were fit to the joint articular surfaces of the bones (i.e., glenoid, proximal and distal humerus) in Meshmixer (Autodesk Inc., San Rafael, CA, USA). 3D models of the bones, muscles, muscle insertion sites and joint primitives were imported into Maya (versions 2019, 2020, Autodesk Inc., San Rafael, CA, USA) as.obj files for further analysis and construction of the biomechanical models. In Maya, centroids of the muscle attachment meshes were calculated using the "vertAvg" tool from the XROMM toolbox (available at https://bitbucket.org/xromm/xromm_mayatools/wiki/Home). For muscles with more extensive soft-tissue attachments that could not be easily mapped onto bones, e.g. the mm. latissimus dorsi and pectoralis, origin and insertion points were placed manually based on 3D muscle geometry (Fahn-Lai et al., 2020; Regnault and Pierce, 2018). Initial muscle paths were defined as straight lines running from the origin to insertion centroids in Maya, but these were later refined in OpenSim.

Model assembly

To facilitate comparisons across animals with very different habitual postures, all models were initially positioned in a global 'reference pose', at which all joint angles equaled zero (Figure 1). This reference pose and reference joint coordinate system (JCS) generally follows previous studies (Baier and Gatesy, 2013) and was constructed in Maya as follows. The pectoral girdle was first positioned such that it was anatomically aligned with the global axes: the dorsoventral Z-axis corresponds with the direction of gravity, the craniocaudal Y-axis with the animal's direction of travel, and the X-axis is perpendicular to both (see Figure S1). The joint coordinate system for the glenoid is oriented in the same way. The humerus was then aligned with the glenoid such that the humerus' long axis pointed laterally, parallel to the global X-axis, and with the distal humerus parallel to the ground (Figures 1 and S1). In this configuration, glenohumeral joint rotation about the dorsoventrally oriented Z-axis represents humeral retraction (-Z) and protraction (+Z); rotation around the craniocaudally oriented Y-axis represents humeral depression (-Y) and elevation (+Y); and rotation about the mediolaterally oriented X-axis represents humeral long-axis rotation (pronation +X and supination -X) (Figure 1). Protraction-retraction and elevation-depression are akin to longitude and latitude on a sphere, and long-axis rotation denotes the heading (Manafzadeh and Gatesy, 2020). The elbow joint was oriented so that the global zero was an extended pose, with the long axis of the antebrachium parallel to the horizontal plane (Figures 1 and S1).

The joint rotation terminology used here deviates from previous *in vivo* locomotion studies, which tend to refer to "flexion-extension" and "abduction-adduction". However, these studies typically do not consider sprawling and parasagittal taxa within the same experimental design, and so the same terms often describe very different joint and limb movements. For instance, "flexion-extension" as traditionally used describes movement of limb in the horizontal plane in a sprawling animal and the vertical plane in a parasagittal animal. Therefore, we developed a standardized joint coordinate system that can be applied across the sprawling–parasagittal postural continuum. From the reference pose with the thumb pointed cranially (Figure 1), glenohumeral joint rotations result in the following movements: protraction brings the elbow cranially (comparable to sprawled extension and parasagittal abduction) and retraction brings the elbow caudally (comparable to sprawled flexion and parasagittal adduction); elevation brings the elbow dorsally (comparable to sprawled abduction and parasagittal flexion) and depression brings the elbow ventrally (comparable to sprawled adduction and parasagittal extension); pronation (internal rotation) rotates the thumb downwards and supination (external rotation) rotates the thumb upwards.

Separate from the global reference pose, we also set up an anatomically informed 'neutral pose', based on joint anatomy, which was distinct for each animal (Figure 1). Based on comparison with experimental data (Jenkins, 1970; Jenkins and Goslow, 1983; Jenkins and Weijs, 1979; Pridmore, 1985), each neutral pose was considered representative of a pose the animals might use in life and was used as the 'starting pose' during the ROM analysis. However, all angles were measured relative to the reference pose, using the globally oriented reference JCS. To generate the neutral pose, local anatomical axes were created in Maya and aligned based on the articular surface morphology of the shoulder joint (glenoid and humeral head) (Figure S2). For the proximal portion of the shoulder joint, plane primitives were fit to the glenoid and the X-axis was oriented normal to the fitted plane. The Y and Z-axes were then aligned so that, when articulated, the surface of humerus covered by the attachments for the elbow extensor musculature - the "extensor" surface, see Fahn-Lai et al. (2020) - faced dorsally (Figure S2, top row). For the distal portion of the shoulder

joint, convex hulls were fit to the articular surface of the humeral head in Meshmixer and imported into Maya. These convex hulls approximated hemi-spheres or hemi-ellipsoids, and so the Y and Z-axes were positioned in the plane of the base of the convex hull and the X-axis was oriented such that it passed through the "pole" (Figure S2, middle row). The Y-axis was aligned with the cranio-caudal axis of the humeral head (assuming the humerus is in the reference pose), and the Z-axis was perpendicular to both (Figure S2, middle row). The proximal and distal anatomical glenohumeral axes were then superimposed, and joint spacing adjusted by translating the humerus along the anatomical X-axis, oriented normal to the glenoid (Figure S2, bottom row). For all three taxa, minimum joint spacing – assessed by extruding the humeral head until it contacted the glenoid – was less than 1% humeral length. This spacing matched well with spacing observed in the CT scans, and in previous modelling studies (Regnault and Pierce, 2018). Once the joints were appropriately aligned and spaced, we defined the glenohumeral joint's center of rotation as the position of the distal anatomical axis in neutral pose; centered in the basal plane of the hemi-spherical (or hemi-ellipsoidal) convex hull for the humeral head (Figure S2, bottom row). The reference joint coordinate system was then translated to this position while keeping its global orientation, and all glenohumeral joint angles were measured using this reference JCS, relative to the reference pose.

For the elbow, we used the same global axis system, but the joint was flexed at 90° for the anatomically informed starting pose, with the joint center defined as the center of a cylinder primitive fit to the distal humerus articular surfaces.

QUANTIFICATION AND STATISTICAL ANALYSIS
Estimating and analyzing range of motion (ROM)

Osteological range of motion (ROM) was measured in Maya, by modifying published automated methods (Manafzadeh and Padian, 2018). Starting from the anatomically aligned neutral pose, the glenohumeral joint was moved through a series of rotation combinations – protraction-retraction angle ±90°, elevation-depression angle ±90°, long-axis rotation angle ±90°, in that rotation order – with increments of 10° (totaling 6,859 poses). We chose to only sample within ±90° of the starting pose rather than sampling all possible poses because many regions of pose space, while osteologically viable, are not biologically realistic and could greatly impact the behaviour of the musculoskeletal models (Manafzadeh and Gatesy, 2021; Manafzadeh and Padian, 2018; Regnault and Pierce, 2018). Surveying published *in vivo* data, animals rarely move their limbs through joint excursions >90° during quadrupedal locomotion (Baier and Gatesy, 2013; Jenkins and Goslow, 1983; Jenkins and Weijs, 1979; Nyakatura et al., 2019), and as the anatomical neutral pose should generally fall within *in vivo* range of motion, we would expect these ROM envelopes to capture many poses used in life. We also chose not to include joint translation in our models. Whilst recent work has demonstrated the importance of translation for accurate ROM estimation in hinge-like joints, ROM estimation for non-hinge joints – such as the glenohumeral joint – is much less affected by the omission of translation (Manafzadeh and Gatesy, 2021). Inclusion of joint translation without proper added constraints also has the capacity to greatly expand the estimated ROM envelope far beyond what is biologically realistic (Manafzadeh and Gatesy, 2021). The main aim of this study was to estimate interspecific MMA variation across pose space, and so we sought to avoid including unrealistic poses that could potentially skew our MMA results.

For each combination of joint angles, poses were deemed viable if there was both no bone-to-bone interpenetration, and the joints were still articulated, i.e., if joint surfaces were deemed to overlap (Figure S3). Bone-to-bone intersection and joint articulation were automatically assessed using a set of Boolean intersection operations in Maya. For each species, the complete list of viable poses was exported from Maya as a .csv file. These files were then imported into R for further analysis and visualization. We performed a cosine-correction of our 3D pose space, as this allows more accurate inter-model comparisons and 3D ROM visualizations. The cosine-correction applied here avoids distortion of the ROM envelope by accounting for the non-linear mapping between differences in joint orientation and distance between points in "uncorrected" Euler space (Manafzadeh and Gatesy, 2020). We compared total joint mobility by calculating the volume of alpha shapes or "concave hulls" fitted to the viable poses for each taxon in cosine-corrected pose space using an alpha value of 10 (Manafzadeh and Gatesy, 2020; Manafzadeh and Padian, 2018).

Estimating and analyzing muscle moment arms (MMA)

Information from the Maya scene – bone meshes, joint axis orientation and position, and shoulder muscle insertion and origin position – was converted into an OpenSim (version 4.1) model using a set of

custom-written Python and R scripts. In OpenSim (Delp et al., 2007), additional refinements to the models were made, such as the addition of wrapping surfaces and via points to constrain the muscle lines of action to anatomically realistic paths (Brassey et al., 2017). To check realistic paths were maintained, we used OpenSim's plot function to visualize changes in muscle moment arm with changes in individual joint angles (e.g., retraction-protraction MMA vs retraction-protraction joint angle) and ensured there were no sharp changes in MMA which might indicate a "break" in the muscle's path (e.g., flipping to the wrong side of a wrapping surface). For each species, all viable glenohumeral joint poses were exported from Maya and converted to motion (.mot) files. These motion files were imported into OpenSim, and MMAs calculated about each rotational degree of freedom for each pose. Our approach thus characterizes MMAs across all feasible glenohumeral joint angles, providing a more comprehensive view of muscle function in relation to limb pose and posture. For all glenohumeral joint poses tested, the elbow remained flexed at 90°.

The MMA data were imported into R for analysis and visualization. MMAs were normalized to specimen size by scaling to humeral volume$^{1/3}$; this was chosen over the more commonly used humeral length due to the differing humeral proportions of our three taxa. In particular, the echidna has a relatively short and wide humerus, and so normalizing to humeral length could result in an overestimation of MMAs compared to the tegu and opossum. Going forward, humeral volume is also easily measured on museum specimens, including fossil taxa with unusual humeral proportions, and where more detailed body dimension data might not be available. At each viable pose for each degree of freedom, we calculated the sum of the normalized moment arms in each direction (positive and negative), to compare across species. When calculating the sums, mean MMA values were calculated for muscles with multiple modelled origins and insertions to avoid overrepresentation skewing the summed MMA results. We took means for mm. biceps, mm. coracobrachialis, m. subscapularis (echidna only), m. infraspinatus (echidna only) and m. latissimus dorsi (Regnault and Pierce, 2018). We also took mean MMAs for the middle plus caudal parts of the m. pectoralis, and for the m. deltoideus scapularis plus m. deltoideus acromialis based on similar electrical activation patterns (Jenkins and Goslow, 1983; Regnault and Pierce, 2018). We plotted the distributions of summed normalized muscle moment arms across pose space and compared them between our three taxa. Due to the large number of datapoints, we also summarized the distributions of both summed MMA and individual muscle MMA across pose space using boxplots and density curves.

ROM and MMAsensitivity analyses

Humeral morphology. A previous study using single-axis degree of freedom ROM found that the echidna glenohumeral joint had extremely low ROM, particularly in retraction-protraction (Regnault and Pierce, 2018). ROM is determined by the interaction between the glenoid facet and humeral head and so differences in the morphology of either could impact glenohumeral mobility. The echidna possesses a hemi-sellar glenoid, similar to the tegu, and this joint type has been hypothesized to limit glenohumeral mobility (Jenkins, 1993). The echidna also has a derived humeral shape among extant mammals, with flared epiphyses and an widened humeral head with a high aspect ratio (Jenkins, 1970; Pridmore, 1985; Regnault and Pierce, 2018); these aspects of its morphology are convergent with "pelycosaur" and basal therapsid-grade synapsids (Lungmus and Angielczyk, 2021). To assess which aspects of the echidna's bony morphology might limit glenohumeral ROM, we repeated the ROM analysis using modified versions of the echidna model: first we digitally removed the expanded epiphyses, which may conceivably limit ROM through bone-to-bone contact with the pectoral girdle; second, we scaled down the humerus to 75% its width, which reduced the size of the epiphyses and also narrowed the wide humeral head, which might restrict ROM through bony collision with the glenoid.

Monte Carlo simulations. The moment arm estimates derived from our models are sensitive to several different input parameters, e.g., joint spacing, correct placement and alignment of joint axes, and correct determination of muscle origin and insertion points and subsequently muscle paths. To account for these uncertainties, we conducted a set of Monte Carlo simulations to analyze the sensitivity of our overall results to potential errors in moment arm estimation (Wiseman et al., 2021). Simulations were run in R for 1000 iterations, using a custom-written script. For each muscle in each taxon, we perturbed the moment arm by a single random number, allowing the moment arms to deviate up to ±20% from their original values (Wiseman et al., 2021). This 20% is based on the median error rates in MMA estimation from other studies which estimated moment arms in different ways, e.g., model estimates vs. tendon travel data (Brown et al., 2003; Cox et al., 2019). We then summed the moment arms for each muscle across pose space at each iteration of

the Monte Carlo simulations. This process provided us with simulated error margins around our moment arm estimates – effectively a distribution of distributions of moment arms across pose space – which we used to assess the robustness of our overall conclusions based on interspecific moment arm comparisons.

Scapula mobility. Unlike other terrestrial tetrapods, the therian pectoral girdle is highly mobile, and rotation of the scapula contributes substantially to stride length during locomotion (Jenkins and Weijs, 1979; Fischer and Blickhan, 2006). The scapula in our opossum model was set with the scapular spine at ~60° to the horizontal, approximating the *in vivo* position of the scapula at mid-stance (Jenkins and Weijs, 1979). However, to determine how scapular mobility could affect muscle moment arms at the shoulder joint during locomotion, we repeated the analysis of opossum glenohumeral MMAs across pose space in Open-Sim with the scapula at several different pitch angles (30°, 45°, 60°, 75°, 90°). Pitch is the main axis about which the scapula rotates *in vivo*, and the range of angles chosen covered the range of angles seen *in vivo* during opossum locomotion (Jenkins and Weijs, 1979). As we were aiming to simulate changes during loco-motion, the glenohumeral joint axes remained parented to the scapula in the model's kinematic hierarchy, and so kept the same local orientation with respect to the scapula across the different pitch angles tested. The different scapula pitch angles tested also correspond to different parts of the stride, as the scapula begins stance phase more horizontally inclined (30°), but then pitches so it is vertically oriented at the beginning of swing phase (90°).

ADDITIONAL RESOURCES

For interactive, 3D versions of the ROM and MMA results figures, please see the accompanying Shiny web app (https://robert-brocklehurst.shinyapps.io/rom_mma_app/). If the web app is down for whatever reason, R code for the local version of the app is available on Harvard Dataverse (see Data and code availability section). Instructions for locally running the app in R are included in the Methods S1.